

1 Age-dependent effects in the transmission and control of  
2 COVID-19 epidemics

3

4 Authors: Nicholas G. Davies<sup>1\*</sup>, Petra Klepac<sup>1^</sup>, Yang Liu<sup>1^</sup>, Kiesha Prem<sup>1</sup>, Mark Jit<sup>1</sup>, CMMID  
5 COVID-19 working group, Rosalind M Eggo<sup>1\*</sup>

6

7 The CMMID COVID-19 working group<sup>1</sup> is: Carl A B Pearson, Billy J Quilty, Adam J  
8 Kucharski, Hamish Gibbs, Samuel Clifford, Amy Gimma, Kevin van Zandvoort, James D  
9 Munday, Charlie Diamond, W John Edmunds, Rein MGJ Houben, Joel Hellewell, Timothy W  
10 Russell, Sam Abbott, Sebastian Funk, Nikos I Bosse, Fiona Sun, Stefan Flasche, Alicia  
11 Rosello & Christopher I Jarvis. Order of working group determined at random.

12

13 <sup>1</sup>Department of Infectious Disease Epidemiology, London School of Hygiene & Tropical  
14 Medicine, Keppel Street, WC1E 7HT

15 ^ these authors contributed equally

16 \* correspondence to Rosalind M Eggo [r.eggo@lshtm.ac.uk](mailto:r.eggo@lshtm.ac.uk) or Nicholas G Davies

17 [nicholas.davies@lshtm.ac.uk](mailto:nicholas.davies@lshtm.ac.uk)

18

19

## 20 Abstract

21

22 The COVID-19 pandemic has shown a markedly low proportion of cases among  
23 children<sup>1,23,4</sup>. Age disparities in observed cases could be explained by children having lower  
24 susceptibility to infection, lower propensity to show clinical symptoms, or both. We evaluate  
25 these possibilities by fitting an age-structured mathematical model to epidemic data from six  
26 countries. We estimate that clinical symptoms occur in 25% (95% CrI: 19–32%) of infections  
27 in 10–19-year-olds, rising to 76% (68–82%) in over-70s, and that susceptibility to infection in  
28 under-20s is approximately half that of older adults. Accordingly, we find that interventions  
29 aimed at children may have a relatively small impact on total cases, particularly if the  
30 transmissibility of subclinical infections is low. The age-specific clinical fraction and  
31 susceptibility we have estimated has implications for the expected global burden of COVID-  
32 19 because of demographic differences across settings: in younger populations, the  
33 expected clinical attack rate would be lower, although it is likely that comorbidities in low-  
34 income countries will affect disease severity. Without effective control measures, regions  
35 with older populations may see disproportionately more clinical cases, particularly in the later  
36 stages of the pandemic.

37

## 38 Main

39 COVID-19 shows an increased number of cases and risk of severe disease with increasing  
40 age<sup>5,6</sup>, a feature shared with the 2003 SARS epidemic<sup>5</sup>. Understanding the role of age in  
41 transmission and disease severity is critical for determining the likely impact of social-  
42 distancing interventions for decreasing transmission, especially those aimed at schools, and  
43 for estimating the expected global disease burden.

44

45 The age gradients in reported cases, observed from the earliest stages of the pandemic,  
46 could be generated by children having decreased susceptibility to infection, decreased

47 probability of showing disease on infection, or a combination of both. A summary of the main  
48 findings, limitations and implications of the model for policy makers is shown in Table 1.  
49

Background	The distribution of confirmed COVID-19 cases has shown strong age dependence, with notably few cases in children. This could be because younger ages are less susceptible to infection and/or are less prone to showing clinical symptoms when infected. We have used dynamic transmission models fitted to a range of available data on the age distribution of reported cases, and to studies that looked for subclinical infections amongst contacts, to estimate the age-specific susceptibility to SARS-CoV-2 infection, and the age-specific fraction of infections that develop clinical symptoms of COVID-19.
Main findings and limitations	We find that under-20s are roughly half as susceptible to infection as over-20s, and that 75% of infections are subclinical in 10–19-year olds, compared to 24% in 70+-year-olds. As with all modelling studies, further data generated during the epidemic could change our parameter estimates. Population mixing measured in contact surveys may not be representative of contact patterns made during the early phase of local epidemics. However, our estimates are consistent across countries and intervention contexts.
Policy implications	These results have implications for the likely effectiveness of school closures in mitigating SARS-CoV-2 transmission, in that these may be less effective than for other respiratory infections. They also have implications for the global expected burden of clinical cases; countries with a large number of children may need to account for decreased susceptibility and severity in burden projections.

50 Table 1. Policy Summary

51  
52 Age-varying susceptibility to infection by SARS-CoV-2, where children may be less  
53 susceptible to becoming infected on contact with an infectious person, would reduce cases  
54 among children, and potentially lower transmission in the population overall. Decreased  
55 susceptibility could result from immune cross-protection from other coronaviruses<sup>8,9,10</sup>, or  
56 possibly from non-specific protection resulting from recent infection by another respiratory  
57 virus<sup>11</sup>, which children experience more frequently than adults<sup>12,13</sup>.  
58  
59 It is also possible that children may experience mild or no symptoms on infection more  
60 frequently than adults. Such age-dependent variation in severity has been observed for other  
61 respiratory virus infections<sup>14</sup>, including SARS<sup>14,15</sup>. For COVID-19, there are indications of age  
62 dependence in severity<sup>8</sup> and mortality<sup>15</sup> among reported cases<sup>15</sup>, which could extend to

63 severity and likelihood of clinically reportable symptoms given infection. “Asymptomatic”  
64 cases have no symptoms at all, and “paucisymptomatic” is sometimes used for those with  
65 very mild symptoms that may not be noticed or reported, even though they occur. We call  
66 these two types “subclinical”, which are more likely to remain undetected than clinically  
67 apparent cases. If subclinical infections exhibit age dependence there would be lower  
68 reported cases among children, but children could still be capable of transmitting the virus to  
69 others, potentially at lower rates than individuals exhibiting clinical infections, as has been  
70 shown for influenza<sup>16</sup>.

71

72 Contact patterns and demographics affect the expected number of cases in each age group.  
73 Children tend to make more social contacts than adults<sup>17</sup> and hence, all else equal,  
74 contribute more to transmission than adults<sup>18,19</sup>. This is why school closures are considered  
75 a key intervention for epidemics of respiratory infections<sup>8</sup>, but the impact of school closure  
76 depends on the role of children in transmission.

77

78 The particular context of SARS-CoV-2 emergence in Wuhan, China, could have resulted in a  
79 skewed age distribution because early cases were in older adults<sup>20</sup>, and assortative mixing  
80 between adults could have reduced transmission to children in the very early stages of the  
81 outbreak, with subsequent closure of schools on 12th January 2020 for the Lunar New Year  
82 holiday potentially reinforcing this effect. Outside of China, COVID-19 outbreaks may have  
83 been initially seeded by working-age travellers entering the country<sup>21,22</sup>, producing a similar  
84 excess of older individuals in early phases of local epidemics.

85

86 Determining the role of children in transmission using available data has important  
87 implications for policies that aim to control transmission<sup>23</sup>, especially through interrupting  
88 child-driven transmission. Additionally, if the number of infections or cases depends strongly  
89 on the role of children, countries with different age distributions could exhibit substantially  
90 different epidemic profiles and overall impact of COVID-19 epidemics.

91  
92 We used an age-stratified transmission model with heterogeneous contact rates between  
93 age groups to examine varying susceptibility to infection by age; varying clinical fraction by  
94 age; and no age variation in susceptibility or clinical fraction (see Methods). We generated  
95 model variants (**Fig 1a**) and fitted each to data sources from the epidemic in Wuhan: a time  
96 series of reported cases<sup>1</sup> and four snapshots of the age distribution of cases<sup>124</sup> (**Fig 1;**  
97 **Extended Data Figure 1**). We included the observed school closures, which decreased the  
98 school contacts of children in the model. We also estimated the effect of the Lunar New Year  
99 holiday period, and the travel and movement restrictions in Wuhan, on transmission (**Fig**  
100 **1d**). We found that under each hypothesis, the basic reproduction number  $R_0$  was 2.5-2.8  
101 initially, was inflated 1.2–1.4-fold during the pre Lunar New Year holiday period, and then fell  
102 by 60–70% during restrictions in Wuhan (**Fig 1e**).

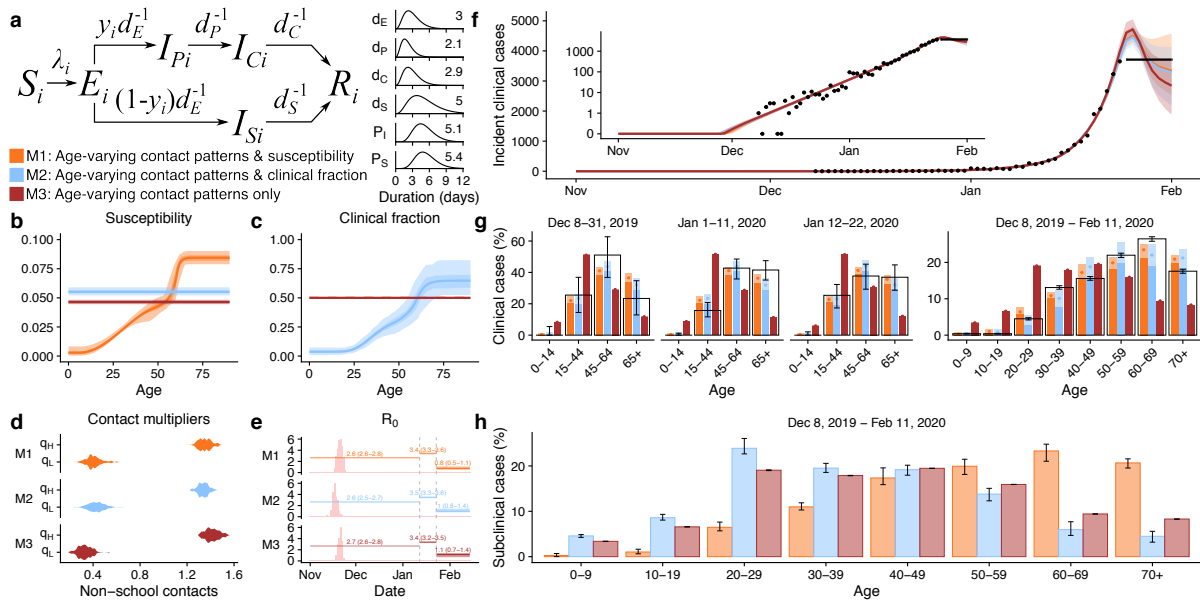
103  
104 All model variants fitted the daily incident number of confirmed cases equally well (**Fig 1f**),  
105 but the model without age-varying susceptibility or clinical fraction could not reproduce the  
106 observed age distribution of cases, overestimating the number of cases in children and  
107 underestimating cases in older adults (**Fig 1g**). The other two fitted the observed age  
108 distribution of cases, but the model assuming no age variation in clinical fraction implied a  
109 large number of mild or asymptomatic infections among the elderly (**Fig 1h**). Comparison  
110 using Deviance Information Criterion<sup>6</sup> (DIC) showed that age varying susceptibility (DIC:  
111 697) and age-varying clinical fraction (DIC: 663) were preferred over the model with neither  
112 (DIC: 976).

113  
114 In the model with age-varying susceptibility, 20% of infections occurred in over-70s, with half  
115 of these as clinical cases, and the other half as subclinical infections (**Fig 1h**). In the model  
116 with age-varying clinical fraction, 20% of infections occurred in over-70s, but less than a  
117 quarter of these were subclinical. Recent work has demonstrated an age-dependent severity

118 in hospitalised confirmed cases<sup>25,26</sup>, which suggests that subclinical infection in older adults  
 119 may be rare and supports the clinical fraction increasing with age.

120

121



122

123

124

125

126

127

128

129

130

131

132

133

134

135

136

137

138

139

140

141

142

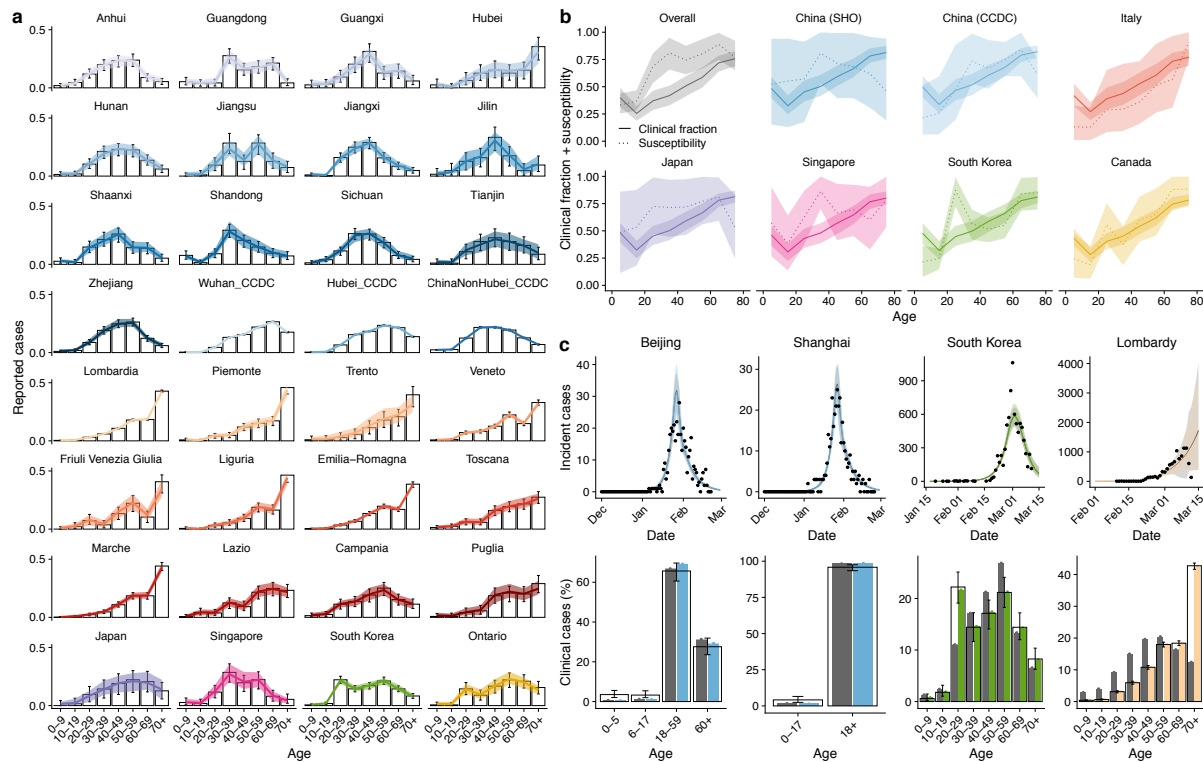
143

144

**Fig. 1. Comparing the fit of different model variants to data from Wuhan City, China. (a)** Model diagram showing duration of disease states in days, where  $d$  parameters represent the duration of time in each disease state,  $y_i$  is the fraction of infections that are clinical in age group  $i$ ,  $\lambda_i$  is the force of infection in age group  $i$ ,  $P_i$  is the incubation period and  $P_s$  is the serial interval (see Methods). **(b)** Susceptibility by age for the three models. Age-specific values were estimated for model 1 (orange). Susceptibility is defined as the probability of infection on contact with an infectious person. **(c)** Clinical fraction ( $y_i$ ) by age for the three models. Age-specific values were estimated for model 2 (blue), and fixed at 0.5 for models 1 and 3. **(d)** Fitted contact multipliers for holiday ( $q_H$ ) and restricted periods ( $q_L$ ) for each model showed an increase in non-school contacts beginning on January 12th (start of Lunar New Year) and a decrease in contacts following restrictions on January 23rd. **(e)** Estimated  $R_0$  values for each model. The red barplot shows the inferred window of spillover of infection. **(f)** Incident reported cases (black), and modelled incidence of reported clinical cases for the three models fitted to cases reported by China Centers for Disease Control (CCDC)<sup>1</sup> with onset on or before February 1st, 2020. Line marks mean and shaded window is the 95% highest density interval (HDI). **(g)** Age distribution of cases by onset date as fitted to the age distributions reported by Li et al<sup>24</sup> (first three panels) and CCDC<sup>1</sup> (fourth panel). Data are shown in the hollow bars, and model predictions in filled bars, where the dot marks the mean posterior estimate. **(h)** Implied distribution of subclinical cases by age for each model. Credible intervals on modelled values show the 95% HDIs; credible intervals on data for panels g and h show 95% HDIs for the proportion of cases in each age group.

145 It is possible that both age-varying susceptibility and age-varying clinical fraction contribute  
146 to some degree to the observed age patterns. To investigate this possibility, we fitted a  
147 model in which both susceptibility and clinical fraction varied by age, estimating these  
148 parameters across 32 settings in six countries. We fitted the stationary distribution of the  
149 next generation matrix to reproduce the locally-reported age distribution of cases compiled  
150 from a variety of sources (**Fig 2a**) and jointly fitted data from five recent studies giving  
151 information on infection rates and symptom severity across ages<sup>25,27–30</sup> (**Extended Data**  
152 **Figure 2**). We used setting-specific demographics, measured contact matrices where  
153 possible, and synthetic contact matrices otherwise (see Methods)<sup>31</sup>. The age-dependent  
154 clinical proportion was markedly lower in younger age groups in all regions (**Fig 2b**), with  
155 25% (19–32%) of infections in 10–19-year-olds resulting in clinical cases, rising to 76% (68–  
156 82%) in adults over 70 in the consensus age distribution estimated across all regions; the  
157 age-specific susceptibility profile suggested that under-20s were half as susceptible to  
158 SARS-CoV-2 infection as over-20s (**Extended Data Table 1**). To determine whether this  
159 distribution was capable of reproducing epidemic dynamics, we fitted our dynamic model to  
160 the incidence of clinical cases in Beijing, Shanghai, South Korea and Italy (**Fig 2c**;  
161 **Extended Data Figure 3**). The consensus age-specific clinical fraction was largely capable  
162 of reproducing the age distribution of cases, although there are some outliers, for example in  
163 the 20–29 age group in South Korea. This could be the result of clustered transmission  
164 within a church group in this country<sup>4</sup>. The predicted age distribution of cases for Italy is also  
165 less skewed towards older adults than reported cases show, suggesting potential differences  
166 in age-specific testing in Italy<sup>32</sup>. Locally-estimated age-varying clinical fraction captured  
167 these patterns more precisely (**Fig. 2c**).

168



169  
170  
171  
172  
173  
174  
175  
176  
177  
178

**Fig 2. Estimating age-specific symptomatic rate from age-specific case counts for 6 countries.**

(a) Age-specific reported cases from 13 provinces of China, 12 regions of Italy, Japan, Singapore, South Korea, and Ontario, Canada. Hollow bars are data and colour is model fit with 95% HDI. (b) Fitted mean and 95% HDI for the age distribution in clinical fraction (solid lines) and age distribution of susceptibility (dashed lines) for all countries. The overall consensus fit is shown in grey. (c) Fitted incidence of confirmed cases and resulting age distribution of cases using either the consensus (grey) or country-specific (colour) age-specific clinical fraction from b.

179 School closures during epidemics<sup>33,34</sup> and pandemics<sup>35,36</sup> aim to decrease transmission  
180 amongst children<sup>18</sup>, and may also have whole-population effects if children play a major role  
181 in transmission. The impact will depend on the fraction of the population that are children,  
182 the contacts they have with other age groups, their susceptibility to infection, and  
183 infectiousness if infected. Using schematic values for pandemic influenza<sup>37</sup> and our inferred  
184 values for COVID-19 (**Figure 3a**) we compared epidemics in three cities with very different  
185 demography: Milan (Italy, high median age), Birmingham (UK, intermediate median age),  
186 and Bulawayo (Zimbabwe, low median age) (**Fig 3b**), using measured contact matrices for  
187 each country. There were many more clinical cases for COVID-19 than influenza in all cities  
188 (mean attack rate across three cities: 361 per 1000 for COVID-19 versus 23 per 1000 for  
189 influenza), with relatively more cases occurring in under-20s (68%) in the influenza-like



190 scenario compared to COVID-19 (17%) (**Fig 3c**). More clinical cases were in older adults in  
191 Milan compared with the other cities, and a markedly younger age distribution was observed  
192 for clinical cases in Bulawayo. The age distribution of clinical cases depends on the  
193 demography and mixing in the region.

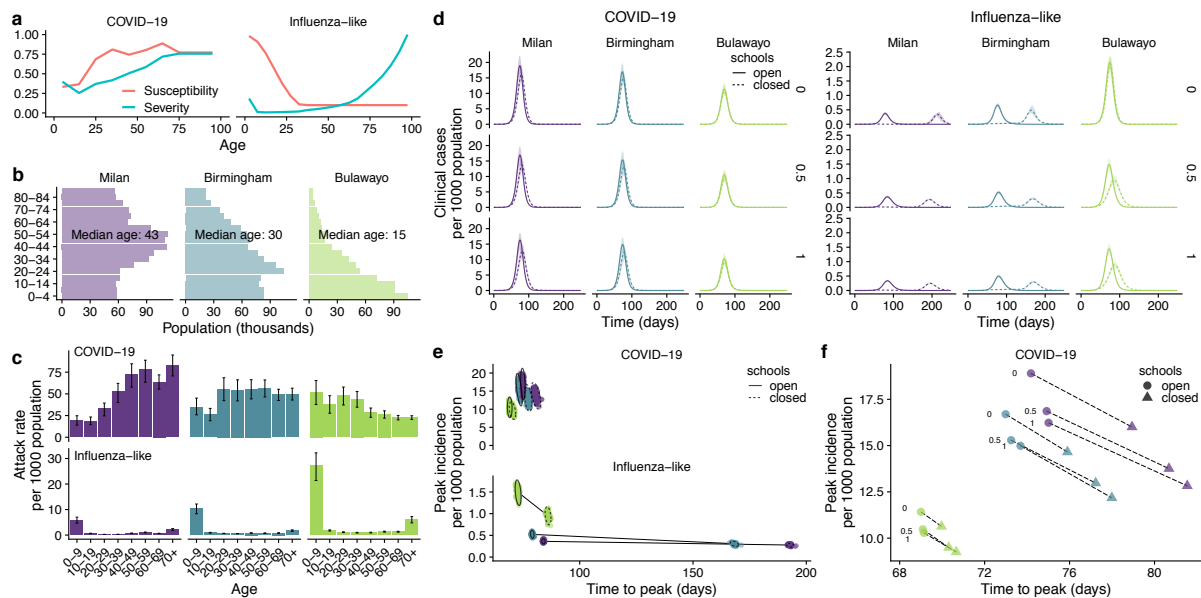
194

195 To explore the effect of school closure, we simulated 3 months of school closures with  
196 varying infectiousness of subclinical infections, at either 0%, 50% or 100% the  
197 infectiousness of clinical cases (**Fig 3d**). For influenza- like infections we found that school  
198 closures decreased peak incidence by 17–35% across settings, and delayed the peak by 10-  
199 89 days across settings (**Fig 3e**). For COVID-19 epidemics, the delay and decrease of the  
200 peak was smaller (9–18% decrease in peak incidence, 1–6 day delay in peak timing),  
201 especially in Bulawayo, which has the highest proportion of children (**Fig 3e**). Because  
202 children have lower susceptibility and exhibit more subclinical cases for COVID-19, school  
203 closures were slightly more effective at reducing transmission of COVID-19 when the  
204 subclinical infectiousness was assumed to be higher (school closures were 37–53% more  
205 effective at reducing peak cases across settings for 100% versus 0% subclinical  
206 infectiousness) (**Fig 3f**).

207

208

209



210

211

212

213

214

215

216

217

218

219

220

221

222

**Fig. 3. Effect of school closure under different demographics and subclinical infectiousness.** (a) Age dependence in clinical fraction (severity) and susceptibility to infection on contact for COVID-19, and for the influenza-like scenarios (simplified, based on ref. <sup>37</sup>) considered here. (b) Age structure for the 3 exemplar cities. (c) Age-specific attack rate for COVID-19 and influenza-like infections, assuming 50% subclinical infectiousness. (d) Daily incidence of clinical cases in exemplar cities for COVID-19 versus influenza-like infections.  $R_0$  is fixed at 2.4. The rows show the impact of varying the infectiousness of subclinical infections to be 0%, 50%, or 100% as infectious as clinical cases while keeping  $R_0$  fixed. (e) Change in peak timing and peak cases for the three cities, for either COVID-19 or influenza-like. (f) Change in median COVID-19 peak timing and peak cases for the three cities, depending on the infectiousness of subclinical infections.

223

224

225

226

227

228

229

230

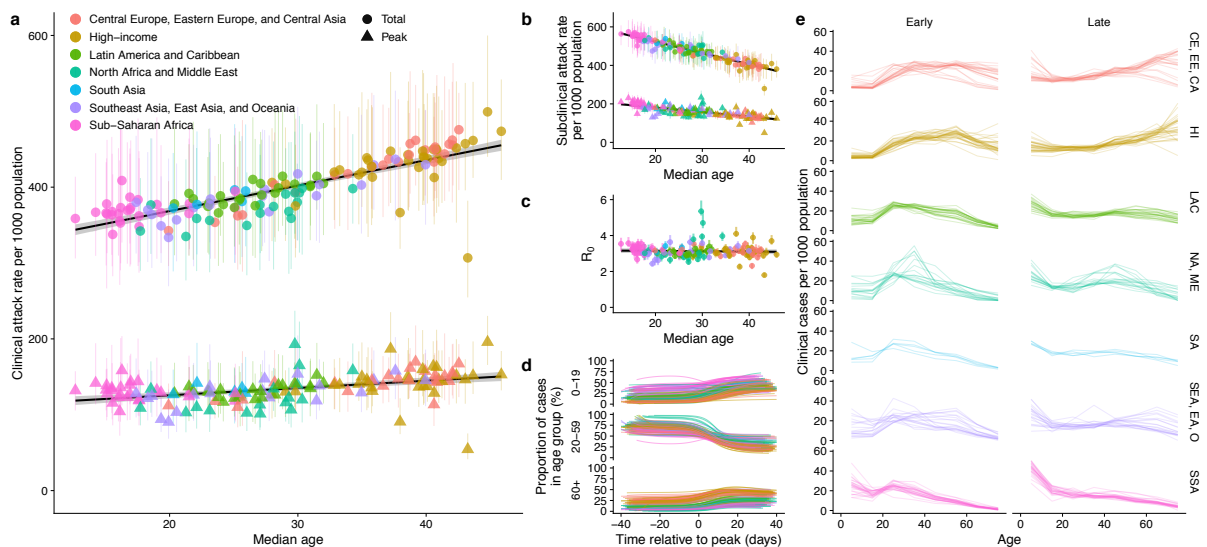
231

232

Age dependence in susceptibility and clinical fraction has implications for the projected global burden of COVID-19. We simulated COVID-19 epidemics in 146 capital cities and found that the total expected number of clinical cases in an unmitigated epidemic varied between countries depending on the median age of the population, which is a proxy for the age structure of the population. The mean estimated basic reproduction number,  $R_0$ , did not substantially differ by median age (Fig 4c), because although there was a greater proportion of children the susceptibility of children was lower. We applied the same age-dependent clinical fraction to all countries, but the relationship between age and clinical symptoms may be different in different countries, perhaps because of a different distribution of comorbidities<sup>38</sup>, or setting—specific comorbidities such as HIV<sup>39</sup>. If the relationship between

233 clinical fraction and age skews younger in low and lower-middle income countries, there  
 234 would be higher clinical attack rates in these countries (**Extended Data Figure 4**).  
 235  
 236 The expected age distribution of cases shifted substantially during the epidemic, where in  
 237 the early phase there were more cases in the central age group (20-59), and after the peak a  
 238 higher proportion on cases in younger and older ages (**Fig 4d**). The size of the shift was  
 239 higher in countries with higher median age, which impacts projections for likely healthcare  
 240 burdens at different phases of the epidemic (**Fig 4e**), particularly because older individuals  
 241 tend to have higher healthcare utilisation if infected<sup>1</sup>.

242  
 243



244  
 245 **Fig. 4. Implications for global preparedness.** (a) Expected clinical case attack rate (mean and 95%  
 246 HDI), and peak in clinical case incidence for 146 countries in the Global Burden of Disease (GBD)  
 247 country groupings<sup>40</sup> for an unmitigated epidemic. (b) Expected sub clinical case attack rate, and peak  
 248 in subclinical cases. (c) Estimated basic reproduction number ( $R_0$ ) in the capital city of each country  
 249 assuming age-specific clinical fraction shown in Fig. 2b and 50% infectiousness of subclinically  
 250 infected people. (d) Proportion of clinical cases in each age group at times relative to the peak of the  
 251 epidemic. The 146 city epidemics were aligned at the peak, and colours mark the GBD groupings in  
 252 a. (e) Age distribution of the first third and last third of clinical cases for 146 countries in GBD  
 253 groupings.

254  
 255 We have shown age dependence in susceptibility to infection and in the probability of  
 256 displaying clinical symptoms of COVID-19, from around 20% in under 10s, to over 70% in  
 257 older adults. For a number of other pathogens, there is evidence that children (except for the

258 very youngest) have lower rates of symptomatic disease<sup>12</sup> and mortality<sup>26</sup>, so the variable  
259 age-specific clinical fraction for COVID-19 we find here fits with other studies. We have  
260 quantified the age-specific susceptibility from available data, and other study types will be  
261 needed to build the evidence base for the role of children, including serological surveys, and  
262 close follow up of infected households.

263

264 The age-specific distribution of clinical infection we have found is similar in shape (but larger  
265 in scale) to that generally assumed for pandemic influenza, but the age-specific susceptibility  
266 is inverted. These differences have a large effect on how effective school closures may be in  
267 limiting transmission, delaying the peak of expected cases, and decreasing the total and  
268 peak number of cases. For COVID-19, school closures are likely to be much less effective  
269 than for influenza-like infections.

270

271 It is critical to determine how infectious subclinical infections are compared to clinical  
272 infections in order to properly assess predicted burdens both with and without interventions.

273 It is biologically plausible that milder cases are less transmissible, for example, because of  
274 an absence of cough<sup>28,29</sup>, but direct evidence is limited<sup>41</sup> and viral load is high in both clinical  
275 and subclinical cases<sup>30</sup>. If those with subclinical infection are efficient transmitters of infection  
276 compared to those with clinical infections, the overall burden is higher than if they are not as  
277 infectious. At the same time, lower relative infectiousness would reduce the impact of  
278 interventions targeting younger ages, such as school closure. By analysing epidemic  
279 dynamics before and after school closures, or close follow up in household studies, it may be  
280 possible to estimate the infectiousness of subclinical infections, however this will rely on  
281 granular data by age and time.

282

283 A great deal of concern has been directed toward the expected burden of COVID-19 in low  
284 and middle income countries (LMIC), which have lower population median age than many  
285 high income countries. Our results show that these demographic differences, coupled with a

286 lower susceptibility and clinical fraction in younger ages, can result in proportionally fewer  
287 clinical cases than would be expected in higher-income countries with flatter demographic  
288 pyramids. This should not be interpreted as few cases in LMIC, because the projected  
289 epidemics are still very large, resulting in high numbers infected. Moreover, the particular  
290 relationships found between age, susceptibility, and clinical fraction are drawn from high and  
291 middle income countries and may reflect not only age, but also the increasing frequency of  
292 comorbidities with age. This relationship may therefore differ in LMIC for two key reasons:  
293 first, the distribution of non-communicable comorbid conditions—which are already known to  
294 increase the risk of severe disease from COVID-19<sup>15</sup> may be differently distributed by age,  
295 often occurring in younger age groups<sup>40</sup>, along with other possible risk factors such as  
296 undernutrition<sup>42</sup>; and second, communicable comorbidities such as HIV<sup>39</sup>, TB coinfection  
297 (which has been suggested to increase risk<sup>43</sup>), and others<sup>44</sup> may alter the distribution of  
298 severe outcomes by age. Observed severity and burden in LMIC may also be higher due to  
299 a lack of health system capacity for intensive treatment of severe cases.

300

301 There are some limitations to the study. While information drawn from the early stages of the  
302 epidemic is subject to uncertainty, age-specific information is drawn from several regions  
303 and countries, and clinical studies support the hypothesis presented here. We assumed that  
304 clinical cases are reported at a fixed fraction throughout the time period, although there may  
305 have been changes in reporting and testing practices that affected case ascertainment by  
306 age. We assumed that subclinical infections were less infectious than clinical infections, and  
307 tested the impact of this on our findings (**Extended Data Figures 5 and 6**) but were not able  
308 to estimate how infectious subclinical infections were. The sensitivity analyses showed very  
309 similar clinical fraction and susceptibility with age, and we demonstrated the effect of this  
310 parameter on school closure and global projections (**Fig. 3, Extended Data Figure 6**). We  
311 have used mixing matrices from the same country, but not the same location as the fitted  
312 data. We used contact matrices that combined physical and conversational contacts. We  
313 therefore implicitly assume that they are a good reflection of contact relevant for the

314 transmission of SARS-CoV-2. If fomite, or faecal-oral routes of transmission are important in  
315 transmission, these contact matrices may not be representative of transmission risk.

316

317 The role of age in transmission is critical to designing interventions aiming to decrease  
318 transmission in the population as a whole, and to projecting the expected global burden.  
319 Early evidence<sup>25</sup>, including presented here, suggests that there is age dependence in  
320 susceptibility and in the risk of clinical symptoms following infection. Understanding if and by  
321 how much subclinical infections contribute to transmission has implications for predicted  
322 global burden and the impact of control interventions. This question must be resolved to  
323 effectively forecast and control COVID-19 epidemics.

324

## 325 Methods

326

### 327 **Transmission model structure used in all analyses**

328 We use an age-structured deterministic compartmental model (Fig. 1a, main text) stratified  
329 into 5-year age bands, with time approximated in discrete steps of 0.25 days. Compartments  
330 in the model are stratified by infection state (S, E,  $I_P$ ,  $I_C$ ,  $I_S$ , or R), age band, and the number  
331 of time steps remaining before transition to the next infection state. We assume that people  
332 are initially susceptible (S), and become exposed (E) after effective contact with an  
333 infectious person. After a latent period, exposed individuals either develop a clinical or  
334 subclinical infection; an exposed age- $i$  individual develops a clinical infection with probability  
335  $y_i$ , otherwise developing a subclinical infection. Clinical cases are preceded by a preclinical  
336 but infectious ( $I_P$ ) state; from the preclinical state, individuals develop full symptoms and  
337 become clinically infected ( $I_C$ ). Based on evidence for other respiratory infections<sup>16</sup> we  
338 assume that subclinical infections ( $I_S$ ) are less infectious compared to preclinical and clinical  
339 infections, and that subclinical individuals remain in the community until they recover. We  
340 use 50% as a baseline for the relative infectiousness of individuals in the subclinical state,  
341 and test the impact of other values (**Extended Data Figs. 5 and 6**). Isolated and recovered  
342 individuals eventually enter the removed state (R); we assume these individuals are no  
343 longer infectious and are immune to reinfection.

344

345 The length of time individuals spend in states E,  $I_P$ ,  $I_C$ , or  $I_S$  is distributed according to  
346 distributions  $d_E, d_P, d_C$ , or  $d_S$ , respectively (**Extended Data Table 2**). The force of infection  
347 for an individual in age group  $i$  at time  $t$  is

$$348 \quad \lambda_{i,t} = u_i \sum_j c_{ij,t} (I_{Pj} + I_{Cj} + f I_{Sj}) / N_j,$$

349 where  $u_i$  is the susceptibility to infection of an age- $i$  individual,  $c_{ij,t}$  is the number of age- $j$   
350 individuals contacted by an age- $i$  individual per day at time  $t$ ,  $f$  is the relative infectiousness  
351 of a subclinical case, and  $(I_{Pj} + I_{Cj} + f I_{Sj}) / N_j$  is the effective probability that a random age- $j$

352 individual is infectious. Contacts vary over time  $t$  depending upon the modelled impact of  
353 school closures and movement restrictions (see below).

354

355 To calculate the basic reproductive number,  $R_0$ , we define the next generation matrix as

$$356 \quad NGM_{ij} = u_i c_{ij,t} (y_j E(d_P + d_C) + (1 - y_j) f E(d_S)) .$$

357  $R_0$  is the absolute value of the dominant eigenvalue of the next generation matrix.

358

359 We use the local age distribution for each city or region being modelled, and synthetic or  
360 measured contact matrices for mixing between age groups (**Extended Data Table 2**). The  
361 mixing matrices have four types of contacts: home, school, work and other contacts.

362

### 363 **Comparing models by fitting to the Wuhan epidemic**

364 We contrasted three models. In model 1, susceptibility varied by age ( $u_i = u(i)$ ), but the  
365 proportion of exposed individuals who became clinical cases did not vary ( $y_i = y$ ). In model  
366 2, the clinical case probability varied by age ( $y_i = y(i)$ ), but susceptibility did not ( $u_i = u$ ). In  
367 model 3, there were no age-related differences in susceptibility or clinical fraction ( $u_i = u$ ,  
368 and  $y_i = y$ ). Susceptibility and clinical fraction curves were fitted using three control points  
369 for young, middle, and old age, interpolating between them with a half-cosine curve (see  
370 below for details).

371

372 We assumed that the initial outbreak in Wuhan was seeded by introducing one exposed  
373 individual per day of a randomly drawn age between  $A_{\min}$  and  $A_{\max}$  for 14 days starting on a  
374 day ( $t_{\text{seed}}$ ) in November<sup>30,31</sup>. We used the age distribution of Wuhan City prefecture in 2016<sup>45</sup>  
375 and contact matrices measured in Shanghai<sup>32</sup> as a proxy for large cities in China. This  
376 contact matrix is stratified into school, home, work, and other contacts. We aggregated the  
377 last three categories into non-school contacts and estimated how components of the contact  
378 matrix changed early in the epidemic in response to major changes. Schools closed on



379 January 12th for the Lunar New Year holiday, so we decreased school contacts, but the  
380 holiday period may have changed non-school contacts, so we estimate this effect by  
381 inferring the change in non-school contact types,  $q_H$ . Large-scale restrictions started on  
382 January 23rd 2020 giving restrictions on travel and movement imposed by authorities, and  
383 we inferred the change in contact patterns during this period,  $q_L$ . Specifically:

$$384 \quad c_{ij,t} = school(t) \cdot c_{ij|school} + other(t) \cdot c_{ij|other},$$

385 where

$$386 \quad school(t) = \begin{cases} 1 & t < 12 \text{ January} \\ 0 & t \geq 12 \text{ January} \end{cases}$$

388 and

$$389 \quad other(t) = \begin{cases} 1 & t < 12 \text{ January} \\ q_H & 12 \text{ January} \leq t < 23 \text{ January} \\ q_L & t \geq 23 \text{ January.} \end{cases}$$

392  
393 We fitted the model to incident confirmed cases from the early phase of the epidemic in  
394 China (December 8, 2019-February 1, 2020) reported by China CDC<sup>1</sup>. During this period,  
395 the majority of cases were from Wuhan City, and we truncated the data after February 1st  
396 because there were more cases in other cities after this time. We jointly fitted the model to  
397 the age distribution of cases at 3 time windows (December 8, 2019 to January 22, 2020)  
398 reported by Li et al.<sup>24</sup> and a further time window (December 8, 2019 to February 11, 2020)  
399 reported by China CDC<sup>1</sup>. Because there was a large spike of incident cases reported on  
400 February 1 determined to have originated from the previous week, we amalgamated all  
401 cases from January 25 to February 1, including those in the large spike, into a single data  
402 point for the week. We assumed 10% of clinical cases were reported<sup>19</sup>. We used a Dirichlet  
403 distribution with a flat prior to obtain 95% HDIs for reported case data stratified by age group  
404 for display in figures.

405

406 We used Markov-chain Monte Carlo to jointly fit each hypothesis to the two sets of empirical  
407 observations from the epidemic in Wuhan City, China (**Supplementary Table 1**). We used a

408 negative binomial likelihood for incident cases and a Dirichlet-multinomial likelihood for the  
409 age distribution of cases, using the likelihood

$$410 \quad L = \left( \prod_{k=1}^K \text{NegBinom}(C_k | \text{size} = 200, \text{mean} = c_k) \right) \left( \prod_{m=1}^M \text{DirMultinom}(A_m | \frac{200}{||a_m||} a_m) \right)$$

411 Above,  $C_k$  is the observed incidence on day  $k$  while  $c_k$  is the model-predicted incidence for  
412 day  $k$ , for each of  $K$  days.  $A_m$  is the observed age distribution for time period  $m$  (case counts  
413 for each age group) while  $a_m$  is the model-predicted age distribution for the same period, and  
414  $||a_m||$  is the total number of cases over all age groups in time period  $m$ , measured for  $M$   
415 time periods. We set the precision of each distribution to 200 to capture additional  
416 uncertainty in data points that would not be captured with a Poisson or multinomial likelihood  
417 model.

418

419 For all Bayesian inference (i.e. shown in Figs. 1 and 2), we used differential evolution  
420 Markov chain Monte Carlo<sup>46</sup>, first running numerical optimization to place starting values for  
421 each chain near the posterior mode. We then run 2000-3000 samples of burn-in, and  
422 generate at least 10,000 samples post-burn-in. Recovered posterior distributions, with prior  
423 distributions overlaid, are shown in **Extended Data Fig. 1**. We distinguished fitted models  
424 using Deviance Information Criterion (DIC)<sup>47</sup>.

425

#### 426 **Analysis of the stationary age distribution of cases**

427 To infer age-specific clinical fraction and susceptibility from reported case distributions, we  
428 assumed that reported cases follow the stationary distribution of cases reached in the early  
429 phase of an epidemic. Using our dynamic model would allow modelling any transient  
430 emphasis in the case distribution associated with the age of the individuals who seeded  
431 infection in a given region, but since the age of the true first cases is not generally known,  
432 we used the stationary distribution instead. Specifically, we used Bayesian inference to fit  
433 age-specific susceptibility and clinical fraction to the reported case distribution by first  
434 generating the expected case distribution  $k_i$  from (1) the age-specific susceptibility,  $u_i$ , (2) the

435 age-specific clinical fraction,  $y_i$ , (3) the measured or estimated contact matrix for the country,  
436 and (4) the age structure of the country or region. We then used the likelihood

$$437 \quad L = \text{Multinom}(c_i | k_i),$$

438  
439 where  $c_i$  is the observed case distribution, when fitting to data from a single country or  
440 region. When fitting to a combined set of regions and/or countries, we used the likelihood

$$441 \quad L = \prod_{j=1}^m \text{DirMultinom}(c_{i,j} | sk_{i,j})^{w_j}$$

442 across countries  $j \in \{1, 2, \dots, m\}$  with weights  $w_j$  such that  $\prod_j w_j = 1$ . We weighted<sup>48</sup> each of  
443 the 13 provinces of China in our data set by 1/13, each of the 12 regions of Italy by 1/12, the  
444 three reported case distributions from China CDC by 1/3, and data from South Korea,  
445 Singapore, Japan and Ontario each by 1, then scaled all weights to multiply to 1.

446  
447 The age-specific susceptibility  $u_i$  and age-specific clinical fraction  $y_i$  were estimated by  
448 evaluating the expected case distribution  $c_i$  according to the likelihood functions given  
449 above. It is not possible to identify both  $u_i$  and  $y_i$  from case data alone. Accordingly, we  
450 inferred the age-specific clinical fraction,  $y_i$  from surveillance data from Italy reporting the  
451 age-specific number of cases that were asymptomatic, paucisymptomatic, mild, severe, and  
452 critical<sup>29</sup>. We assumed that asymptomatic and paucisymptomatic infections may be  
453 underascertained relative to mild, severe, and critical cases, and therefore estimated an  
454 “inflation factor”  $z > 1$  giving the number of unascertained asymptomatic or  
455 paucisymptomatic infections for each reported infection in these data. Accordingly, we  
456 applied the likelihood penalty

$$457 \quad P_L = \prod_i \text{Beta} \left( \frac{\text{mild}_i + \text{sev}_i + \text{crit}_i}{z(\text{asymp}_i + \text{pauci}_i) + \text{mild}_i + \text{sev}_i + \text{crit}_i} \mid \alpha = 10000y_i, \beta = 10000(1 - y_i) \right)$$

458 when fitting  $y_i$  in order to constrain the relative shape of the clinical fraction curve by age.

459 Here,  $\text{mild}_i$  is the number of mild cases reported in age group  $i$ ,  $\text{sev}_i$  the number of severe  
460 cases in age group  $i$ , etc. Therefore the age-specific clinical fraction reflected the proportion

461 of infections reported by Riccardo et al. as mild, critical, or severe, relative to an estimated  
462 proportion of asymptomatic and paucisymptomatic infections.

463

464 In order to estimate a value for the inflation factor  $z$  compatible with empirical data on the  
465 severity of infections, we applied a further likelihood penalty when estimating the consensus  
466 fit for clinical fraction and susceptibility in order to match information on age-specific  
467 susceptibility collected from recent contact-tracing studies<sup>25,27,28,30</sup>. A leave-one-out analysis  
468 showed that these additional data allowed the model fitting procedure to converge on a  
469 consistent profile for both  $u_i$  and  $y_i$  (**Extended Data Fig. 2**).

470

471 We extracted age-specific case data from the following sources. For provinces of China, we  
472 used age-specific case numbers reported by China CDC<sup>1</sup> as well as line list data compiled  
473 by the Shanghai Observer<sup>49</sup>. For regions of Italy, we used age-specific case numbers  
474 reported by the Istituto Superiore di Sanità on March 13, 2020<sup>50</sup>. For South Korea, we used  
475 the line list released by Kim et al. based on data from the Korea Centers for Disease Control  
476 and Prevention<sup>22</sup>. For Japan, we used the Open Covid Linelist<sup>51,52</sup>. For Singapore, we used  
477 Singapore Ministry of Health data compiled by Koh<sup>21</sup>. For Ontario, we used data compiled by  
478 the COVID-19 Canada Open Data Working Group<sup>53</sup>.

479

480 To validate our line list analysis, we fitted the dynamic model to incidence data from Beijing,  
481 Shanghai, South Korea and Lombardy, Italy (**Extended Data Fig. 3**). We fixed the reporting  
482 rate for Beijing, Shanghai, South Korea, and Lombardy to 20%. Beijing and Shanghai  
483 incidence data were given by case onset, so we assumed no delay between reported and  
484 true case onsets. Incidence data for South Korea were given by the date of confirmation  
485 only; we assumed the reporting delay followed a gamma distribution with a 7-day mean.  
486 Incidence data for Italy were given separately for case onset and case confirmation, with  
487 only a subset of onset dates available; accordingly, we fit the proportion of confirmed cases  
488 with onset dates and the delay from onset to confirmation. We adjusted the size parameter

489 of the negative binomial distribution used to model case incidence to 10 to reflect greater  
490 variability among fewer data points for these countries than for Wuhan. Beijing and Shanghai  
491 were fitted jointly, with separate dates of introduction but the same fitted susceptibility, large-  
492 scale restriction date and large-scale restriction magnitude. South Korea and Italy were each  
493 fitted separately; we fitted a large-scale restriction date and magnitude for both South Korea  
494 and Italy.

495

496 For both the line list fitting and validation, we assumed that schools were closed in China,  
497 but remained open in South Korea, Japan, Italy, Singapore, and Canada, as schools were  
498 open for the majority of the period covered by the data in the latter five countries.

499

#### 500 **Quantifying the impact of school closure**

501 To determine the impact in other cities with different demographic profiles we used the  
502 inferred parameters from our line list analysis to parameterise our transmission model for  
503 projections to other cities. We chose these to compare projections for a city with a high  
504 proportion of elderly individuals (Milan, Italy); a moderate-aged population (Birmingham,  
505 United Kingdom); and a city in a low-income country with a high proportion of young  
506 individuals (Bulawayo, Zimbabwe). For this analysis, we compared an outbreak of COVID-  
507 19, for which the burden and transmission is concentrated in relatively-older individuals, with  
508 an outbreak of pandemic influenza, for which the burden and transmission is concentrated in  
509 relatively-younger individuals. We assumed that immunity to influenza builds up over a  
510 person's lifetime, such that an individual's susceptibility to influenza infection plateaus at  
511 roughly age 35, and assumed that the severity of influenza infection is highest in the elderly  
512 and in children under 10 years old<sup>37</sup>.

513

514 To model Milan, we used the age distribution of Milan in 2019<sup>54</sup> and a contact matrix  
515 measured in Italy in 2006<sup>11</sup>. To model Birmingham, we used the age distribution of  
516 Birmingham in 2018<sup>55</sup> and a contact matrix measured in the UK in 2006<sup>11</sup>. To model

517 Bulawayo, we used the age distribution of Bulawayo Province in 2012<sup>56</sup> and a contact matrix  
518 measured in Manicaland, Zimbabwe in 2013<sup>57</sup>. We assumed that the epidemic was seeded  
519 by two infectious individuals in a random age group per week for 5 weeks. We scaled the  
520 age-specific susceptibility  $u_i$  by setting the “target” basic reproductive number  $R_0 = 2.4$ , as a  
521 representative example. We also performed a sensitivity analysis where we scaled  $u_i$  to  
522 result in  $R_0 = 2.4$  in Birmingham, and using the same setting for  $u_i$  in all three cities, so that  
523 the actual  $R_0$  changed depending upon contact matrices and demographics used to model  
524 each city. This produced qualitatively similar results (**Extended Data Figure 7**).

525

526 We projected the impact of school closure by setting the contact multiplier for school  
527 contacts  $school(t)$  to 0. Complete removal of school contacts may overestimate the impact of  
528 school closures because of alternative contacts children make when out of school<sup>58</sup>. This will  
529 however give the maximum impact of school closures in the model to demonstrate the  
530 differences.

531

### 532 **Projecting the global impact**

533 To project the impact of COVID-19 outbreaks in global cities, we used mixing matrices from  
534 Prem et al.<sup>31</sup> and demographic structures for 2020 from World Population Prospects 2019 to  
535 simulate a COVID-19 outbreak in 146 global capital cities for which synthetic matrices,  
536 demographic structures and total populations were available. For simplicity, we assumed  
537 that capital cities followed the demographic structure of their respective countries and took  
538 the total population of each capital city from the R package *maps*. For each city, we scaled  $u_i$   
539 to result in an average  $R_0 = 2.4$  in Birmingham, UK, and used the same setting for  $u_i$  for all  
540 cities, so that the realised  $R_0$  would change according to the contact matrices and  
541 demographics for each city. We simulated 20 outbreaks in each city, drawing the age-  
542 specific clinical fraction  $y_i$  from the posterior of the estimated overall clinical fraction from our  
543 line list analysis (Fig. 2), and analysed the time to the peak incidence of the epidemic, the  
544 peak clinical and subclinical incidence of infection, and the total number of clinical and

545 subclinical infections. We took the first third and the last third of clinical cases in each city to  
546 compare the early and late stages of the epidemic.

547

#### 548 **Contact matrices**

549 Wherever possible, we use measured contact matrices (**Supplementary Table 2**). We adapt  
550 each of these mixing matrices, using 5-year age bands, to specific regions of the countries  
551 they were measured in by reprocessing the original contact surveys with the population  
552 demographics of the local regions. The contact matrices and demographics we used for  
553 Figs. 1-3 of the main text are shown in **Extended Data Figure 8**.

554

555 The contact survey in Shanghai<sup>59</sup> allowed respondents to record both individual (one-on-  
556 one) and group contacts, the latter with approximate ages. While individual contacts were  
557 associated with a context (home, work, school, etc.) group contacts were not, and so we  
558 assumed that all group contacts which involved individuals aged 0-19 occurred at school.  
559 We also assumed that group contacts were lower intensity than individual contacts,  
560 weighting group contacts by 50% relative to one-on-one contacts.

561

562 We assumed schools were closed during the epidemic in China (because schools closed for  
563 the Lunar New Year holiday and remained closed), but open in Italy, Singapore, South  
564 Korea, Japan, and Canada, because we used data from the early part of the epidemics in  
565 those countries during which schools were open.

566

#### 567 **Sensitivity analyses**

568 Since the infectiousness of subclinical individuals was not identifiable from data we have  
569 available, in Figure 2 we adopted a baseline estimate of 50% relative to preclinical and  
570 clinical individuals. In **Extended Data Figure 5**, we performed sensitivity analysis by  
571 repeating our model runs with the alternative values for subclinical infectiousness between  
572 0% and 100%. We did not find marked difference in the findings or estimates.

573

574 In Figure 2 we fitted the age distributions of cases in 6 countries jointly to findings from  
575 recent studies on the susceptibility of children. We tested the sensitivity of our findings to the  
576 findings of the other studies by conducting a leave one out sensitivity analysis. The results  
577 are given in **Extended Data Figure 2**, and we did not find major changes to the shape of the  
578 age-dependence in either susceptibility or clinical fraction.

579

580 In Fig. 3, we showed the epidemic in 3 cities with fixed  $R_0$  at 2.4 to illustrate the impact that  
581 demographics alone have on the effectiveness of interventions. This means that higher rates  
582 of contact measured in surveys in Milan and Bulawayo compared to Birmingham were not  
583 included. We also tested the sensitivity of findings on school closure for which we fix  
584 susceptibility  $u_i$  and therefore  $R_0$  varies (**Extended Data Figure 7**). The conclusions  
585 regarding the relative effectiveness of school closures for COVID-19 versus influenza are  
586 similar.

587

588 In Fig. 4, we assumed that the age-specific clinical fraction was the same across all settings,  
589 but we tested the sensitivity of our projections (Figure 4) to the age-specific clinical fraction  
590 used in lower-income countries. However, a higher rate of comorbidities in lower-income  
591 countries could change the age-specific probability of developing clinical symptoms upon  
592 infection. To investigate this possibility, we construct a schematic alternative age-specific  
593 profile of clinical fraction by (1) increasing the age-specific probability of developing  
594 symptoms by 15% for individuals under the age of 20 and (2) shifting the age-specific clinical  
595 fraction for individual over the age of 20 by 10 years older (**Extended Data Figure 4**). We  
596 repeated the analyses with these functions and found increased burden in lower-income  
597 countries, that could exceed the burden of clinical cases in higher-income countries.

598

599 Finally, we repeated our projections for country-specific burdens of COVID-19 assuming  
600 different values for the relative infectiousness of subclinical infections. We found that this



601 had a relatively small impact on the relationship between median age and case burden  
602 across countries (**Extended Data Figure 6**).

603

604

605

606

### 607 **Acknowledgements**

608 We acknowledge the following for funding: NGD: National Institutes of Health Research  
609 (HPRU-2012-10096). PK, YL, KP, MJ: This research was partly funded by the Bill & Melinda  
610 Gates Foundation (INV-003174). PK: This work was funded in part by the Royal Society  
611 under award RP\EA\180004. YL, MJ: This research was partly funded by the National  
612 Institute for Health Research (NIHR) (16/137/109) using UK aid from the UK Government to  
613 support global health research. The views expressed in this publication are those of the  
614 author(s) and not necessarily those of the NIHR or the UK Department of Health and Social  
615 Care. RME: HDR UK (grant: MR/S003975/1).

616

617 The members of the CMMID COVID-19 working group and the funding they acknowledge  
618 are: Carl A B Pearson, Billy J Quilty (NIHR 16/137/109), Adam J Kucharski (Wellcome Trust  
619 grant: 206250/Z/17/Z), Hamish Gibbs (funded by the Department of Health and Social Care  
620 using UK Aid funding and is managed by the NIHR. The views expressed in this publication  
621 are those of the author(s) and not necessarily those of the Department of Health and  
622 SocialCare (ITCRZ 03010), Samuel Clifford (Wellcome Trust grant: 208812/Z/17/Z), Amy  
623 Gimma (Global Challenges Research Fund (GCRF) for the project "RECAP" managed  
624 through RCUK and ESRC (ES/P010873/1), Kevin van Zandvoort (supported by Elrha's  
625 Research for Health in Humanitarian Crises (R2HC) Programme, which aims to improve  
626 health outcomes by strengthening the evidence base for public health interventions in  
627 humanitarian crises. The R2HC programme is funded by the UK Government (DFID), the  
628 Wellcome Trust, and the UK National Institute for Health Research (NIHR), James D  
629 Munday (Wellcome Trust grant: 210758/Z/18/Z), Charlie Diamond (NIHR 16/137/109), W  
630 John Edmunds, Joel Hellewell (Wellcome Trust grant: 210758/Z/18/Z), Timothy W Russel  
631 (Wellcome Trust grant: 206250/Z/17/Z), Sam Abbott (Wellcome Trust grant: 210758/Z/18/Z),  
632 Sebastian Funk (Wellcome Trust grant: 210758/Z/18/Z), Nikos I Bosse, Fiona Sun (NIHR  
633 EPIC grant 16/137/109), Stefan Flasche (Wellcome Trust grant: 208812/Z/17/Z), Alicia  
634 Rosello (NIHR grant: PR-OD-1017-20002), Christopher I Jarvis (Global Challenges  
635 Research Fund (GCRF) project 'RECAP' managed through RCUK and ESRC  
636 (ES/P010873/1)), RMGJH (European Research Commission Starting Grant: #757699).

637

### 638 **Author contributions**

639 RME conceived the study. NGD and RME designed the model with PK, and YL, KP and MJ  
640 providing input. NGD designed the software and inference framework and implemented the  
641 model. YL processed the data. NGD and RME wrote the first draft of the manuscript. All  
642 authors interpreted the results, contributed to writing, and approved the final version for  
643 submission.

644

### 645 **Data Availability and Code Availability**

646 The data used for fitting are publicly available, but will also be made available with the code  
647 in the github repository for the project at <https://github.com/nicholasdavies/covid-age>.  
648 Contact matrix data are available at zenodo<sup>21,22</sup>.

649

### 650 **Competing interests**

651 The authors have no competing interests.

652

### 653 **Additional information**

654 Supplementary Information is available for this paper. Correspondence and requests for  
655 materials should be addressed to Rosalind M Eggo or Nicholas G Davies at  
656 [r.eggo@lshtm.ac.uk](mailto:r.eggo@lshtm.ac.uk) or [nicholas.davies@lshtm.ac.uk](mailto:nicholas.davies@lshtm.ac.uk)

657

658

### 659 **References**

660

- 661 1. Zhang. The epidemiological characteristics of an outbreak of 2019 novel coronavirus diseases  
662 (COVID-19) in China. *Chin. J. Epidemiol.* **41**, 145–151 (20200217).
- 663 2. Sun, K., Chen, J. & Viboud, C. Early epidemiological analysis of the coronavirus disease 2019  
664 outbreak based on crowdsourced data: a population-level observational study. *Lancet Digit.*  
665 *Health* S2589750020300261 (2020) doi:10.1016/S2589-7500(20)30026-1.
- 666 3. D, C. *et al.* The early phase of the COVID-19 outbreak in Lombardy, Italy. *ArXiv200309320 Q-Bio*  
667 (2020).
- 668 4. Shim, E., Tariq, A., Choi, W., Lee, Y. & Chowell, G. Transmission potential and severity of  
669 COVID-19 in South Korea. *Int. J. Infect. Dis.* S1201971220301508 (2020)  
670 doi:10.1016/j.ijid.2020.03.031.
- 671 5. Dong, Y. *et al.* Epidemiological Characteristics of 2143 Pediatric Patients With 2019 Coronavirus  
672 Disease in China. *Pediatrics* e20200702 (2020) doi:10.1542/peds.2020-0702.
- 673 6. Zhao, X. *et al.* Incidence, clinical characteristics and prognostic factor of patients with COVID-19:  
674 a systematic review and meta-analysis.  
675 <http://medrxiv.org/lookup/doi/10.1101/2020.03.17.20037572> (2020)  
676 doi:10.1101/2020.03.17.20037572.
- 677 7. Anderson, R. M. *et al.* Epidemiology, transmission dynamics and control of SARS: the 2002–2003  
678 epidemic. *Philos. Trans. R. Soc. Lond. B. Biol. Sci.* **359**, 1091–1105 (2004).
- 679 8. Nickbakhsh, S. *et al.* Epidemiology of Seasonal Coronaviruses: Establishing the Context for the  
680 Emergence of Coronavirus Disease 2019. *J. Infect. Dis.* jiaa185 (2020) doi:10.1093/infdis/jiaa185.

- 681 9. Kissler, S. M., Tedijanto, C., Goldstein, E., Grad, Y. H. & Lipsitch, M. Projecting the transmission  
682 dynamics of SARS-CoV-2 through the postpandemic period. *Science* eabb5793 (2020)  
683 doi:10.1126/science.abb5793.
- 684 10. Huang, A. T. *et al.* A systematic review of antibody mediated immunity to coronaviruses: antibody  
685 kinetics, correlates of protection, and association of antibody responses with severity of disease.  
686 <http://medrxiv.org/lookup/doi/10.1101/2020.04.14.20065771> (2020)  
687 doi:10.1101/2020.04.14.20065771.
- 688 11. Cowling, B. J. *et al.* Increased Risk of Noninfluenza Respiratory Virus Infections Associated With  
689 Receipt of Inactivated Influenza Vaccine. *Clin. Infect. Dis.* **54**, 1778–1783 (2012).
- 690 12. Tsagarakis, N. J. *et al.* Age-related prevalence of common upper respiratory pathogens, based  
691 on the application of the FilmArray Respiratory panel in a tertiary hospital in Greece: *Medicine*  
692 (*Baltimore*) **97**, e10903 (2018).
- 693 13. Common cold. *nhs.uk* <https://www.nhs.uk/conditions/common-cold/> (2017).
- 694 14. Galanti, M. *et al.* Rates of asymptomatic respiratory virus infection across age groups. *Epidemiol.*  
695 *Infect.* **147**, e176 (2019).
- 696 15. Zhou, F. *et al.* Clinical course and risk factors for mortality of adult inpatients with COVID-19 in  
697 Wuhan, China: a retrospective cohort study. *The Lancet* S0140673620305663 (2020)  
698 doi:10.1016/S0140-6736(20)30566-3.
- 699 16. Van Kerckhove, K., Hens, N., Edmunds, W. J. & Eames, K. T. D. The Impact of Illness on Social  
700 Networks: Implications for Transmission and Control of Influenza. *Am. J. Epidemiol.* **178**, 1655–  
701 1662 (2013).
- 702 17. Mossong, J. *et al.* Social Contacts and Mixing Patterns Relevant to the Spread of Infectious  
703 Diseases. *PLOS Med.* **5**, e74 (2008).
- 704 18. Cauchemez, S., Valleron, A.-J., Boëlle, P.-Y., Flahault, A. & Ferguson, N. M. Estimating the  
705 impact of school closure on influenza transmission from Sentinel data. *Nature* **452**, 750–754  
706 (2008).
- 707 19. Eames, K. T. D., Tilston, N. L., Brooks-Pollock, E. & Edmunds, W. J. Measured Dynamic Social  
708 Contact Patterns Explain the Spread of H1N1v Influenza. *PLoS Comput. Biol.* **8**, e1002425  
709 (2012).

- 710 20. Huang, C. *et al.* Clinical features of patients infected with 2019 novel coronavirus in Wuhan,  
711 China. *The Lancet* **395**, 497–506 (2020).
- 712 21. Koh, A. Singapore COVID-19 Cases. <http://alexkoh.net/covid19/>.
- 713 22. Data Science for COVID-19 (DS4C). <https://kaggle.com/kimjihoo/coronavirusdataset>.
- 714 23. Lipsitch, M., Swerdlow, D. L. & Finelli, L. Defining the Epidemiology of Covid-19 — Studies  
715 Needed. *N. Engl. J. Med.* **0**, null (2020).
- 716 24. Li, Q. *et al.* Early Transmission Dynamics in Wuhan, China, of Novel Coronavirus–Infected  
717 Pneumonia. *N. Engl. J. Med.* NEJMoa2001316 (2020) doi:10.1056/NEJMoa2001316.
- 718 25. Bi, Q. *et al.* *Epidemiology and Transmission of COVID-19 in Shenzhen China: Analysis of 391*  
719 *cases and 1,286 of their close contacts.*  
720 <http://medrxiv.org/lookup/doi/10.1101/2020.03.03.20028423> (2020)  
721 doi:10.1101/2020.03.03.20028423.
- 722 26. Yang, Y. *et al.* *Epidemiological and clinical features of the 2019 novel coronavirus outbreak in*  
723 *China.* <http://medrxiv.org/lookup/doi/10.1101/2020.02.10.20021675> (2020)  
724 doi:10.1101/2020.02.10.20021675.
- 725 27. Zhang, J. *et al.* Age profile of susceptibility, mixing, and social distancing shape the dynamics of  
726 the novel coronavirus disease 2019 outbreak in China. (2020) doi:10.1101/2020.03.19.20039107.
- 727 28. Gudbjartsson, D. F. *et al.* Spread of SARS-CoV-2 in the Icelandic Population. *N. Engl. J. Med.*  
728 NEJMoa2006100 (2020) doi:10.1056/NEJMoa2006100.
- 729 29. Riccardo, F. *et al.* *Epidemiological characteristics of COVID-19 cases in Italy and estimates of the*  
730 *reproductive numbers one month into the epidemic.*  
731 <http://medrxiv.org/lookup/doi/10.1101/2020.04.08.20056861> (2020)  
732 doi:10.1101/2020.04.08.20056861.
- 733 30. Lavezzo, E. *et al.* Suppression of COVID-19 outbreak in the municipality of Vo, Italy. (2020)  
734 doi:10.1101/2020.04.17.20053157.
- 735 31. Prem, K., Cook, A. R. & Jit, M. Projecting social contact matrices in 152 countries using contact  
736 surveys and demographic data. *PLOS Comput. Biol.* **13**, e1005697 (2017).
- 737 32. Onder, G., Rezza, G. & Brusaferro, S. Case-Fatality Rate and Characteristics of Patients Dying in  
738 Relation to COVID-19 in Italy. *JAMA* (2020) doi:10.1001/jama.2020.4683.

- 739 33. Chan, K. P. Control of Severe Acute Respiratory Syndrome in Singapore. *Environ. Health Prev.*  
740 *Med.* **10**, 255–259 (2005).
- 741 34. Lau, J. T. F. Monitoring community responses to the SARS epidemic in Hong Kong: from day 10  
742 to day 62. *J. Epidemiol. Community Health* **57**, 864–870 (2003).
- 743 35. Cauchemez, S. *et al.* School closures during the 2009 influenza pandemic: national and local  
744 experiences. *BMC Infect. Dis.* **14**, 207 (2014).
- 745 36. Cauchemez, S. *et al.* Closure of schools during an influenza pandemic. *Lancet Infect. Dis.* **9**,  
746 473–481 (2009).
- 747 37. Greer, A. L., Tuite, A. & Fisman, D. N. Age, influenza pandemics and disease dynamics.  
748 *Epidemiol. Infect.* **138**, 1542–1549 (2010).
- 749 38. Clark, A. *et al.* How many are at increased risk of severe COVID-19 disease? Rapid global,  
750 regional and national estimates for 2020.  
751 <http://medrxiv.org/lookup/doi/10.1101/2020.04.18.20064774> (2020)  
752 doi:10.1101/2020.04.18.20064774.
- 753 39. Cohen, C. *et al.* Severe Influenza-associated Respiratory Infection in High HIV Prevalence  
754 Setting, South Africa, 2009–2011. *Emerg. Infect. Dis.* **19**, (2013).
- 755 40. IHME. Global Burden of Disease. <http://www.healthdata.org/gbd>.
- 756 41. Williams, C. M. *et al.* Exhaled Mycobacterium tuberculosis output and detection of subclinical  
757 disease by face-mask sampling: prospective observational studies. *Lancet Infect. Dis.*  
758 S1473309919307078 (2020) doi:10.1016/S1473-3099(19)30707-8.
- 759 42. Murray, J. *et al.* Determining the Provincial and National Burden of Influenza-Associated Severe  
760 Acute Respiratory Illness in South Africa Using a Rapid Assessment Methodology. *PLOS ONE*  
761 **10**, e0132078 (2015).
- 762 43. Liu, Y. *et al.* Active or latent tuberculosis increases susceptibility to COVID-19 and disease  
763 severity. <http://medrxiv.org/lookup/doi/10.1101/2020.03.10.20033795> (2020)  
764 doi:10.1101/2020.03.10.20033795.
- 765 44. Cohen, A. L. *et al.* Potential Impact of Co-Infections and Co-Morbidities Prevalent in Africa on  
766 Influenza Severity and Frequency: A Systematic Review. *PLOS ONE* **10**, e0128580 (2015).
- 767 45. National Bureau of Statistics. China Statistical Year Book. (2005-2018).  
768 <http://www.stats.gov.cn/tjsj/ndsj/>.

- 769 46. Braak, C. J. F. T. A Markov Chain Monte Carlo version of the genetic algorithm Differential  
770 Evolution: easy Bayesian computing for real parameter spaces. *Stat. Comput.* **16**, 239–249  
771 (2006).
- 772 47. Spiegelhalter, D. J., Best, N. G., Carlin, B. P. & van der Linde, A. Bayesian measures of model  
773 complexity and fit. *J. R. Stat. Soc. Ser. B Stat. Methodol.* **64**, 583–639 (2002).
- 774 48. Varin, C., Reid, N. & Firth, D. An overview of composite likelihood methods. *Stat. Sin.* **21**, (2011).
- 775 49. Observer, S. Shanghai Observer. COVID-2019 Linelist.  
776 <http://data.shobserver.com/www/datadetail.html?contId=1000895>.
- 777 50. Epicentro. *Bolletino Sorveglianza Integrata COVID-19 12 Marzo 2020 Appendix*.  
778 [https://www.epicentro.iss.it/coronavirus/bollettino/Bolletino-sorveglianza-integrata-COVID-19\\_12-](https://www.epicentro.iss.it/coronavirus/bollettino/Bolletino-sorveglianza-integrata-COVID-19_12-marzo-2020_appendix.pdf)  
779 [marzo-2020\\_appendix.pdf](https://www.epicentro.iss.it/coronavirus/bollettino/Bolletino-sorveglianza-integrata-COVID-19_12-marzo-2020_appendix.pdf).
- 780 51. COVID19\_2020\_open\_line\_list.  
781 [https://docs.google.com/spreadsheets/d/1itaohdPiAeniCXNIntNztZ\\_oRvjh0HsGuJXUJWET008/e-](https://docs.google.com/spreadsheets/d/1itaohdPiAeniCXNIntNztZ_oRvjh0HsGuJXUJWET008/edit?usp=sharing)  
782 [dit?usp=sharing](https://docs.google.com/spreadsheets/d/1itaohdPiAeniCXNIntNztZ_oRvjh0HsGuJXUJWET008/edit?usp=sharing).
- 783 52. Xu, B. *et al.* Open access epidemiological data from the COVID-19 outbreak. *Lancet Infect. Dis.*  
784 S1473309920301195 (2020) doi:10.1016/S1473-3099(20)30119-5.
- 785 53. COVID-19 in Canada. <https://art-bd.shinyapps.io/covid19canada/>.
- 786 54. Milano (Metropolitan City, Italy) - Population Statistics, Charts, Map and Location.  
787 [http://citypopulation.info/en/italy/admin/lombardia/015\\_\\_milano/](http://citypopulation.info/en/italy/admin/lombardia/015__milano/).
- 788 55. Age breakdown of the population of Birmingham - Office for National Statistics.  
789 [https://www.ons.gov.uk/aboutus/transparencyandgovernance/freedomofinformationfoi/agebreakd-](https://www.ons.gov.uk/aboutus/transparencyandgovernance/freedomofinformationfoi/agebreakdownofthepopulationofbirmingham)  
790 [ownofthepopulationofbirmingham](https://www.ons.gov.uk/aboutus/transparencyandgovernance/freedomofinformationfoi/agebreakdownofthepopulationofbirmingham).
- 791 56. Bulawayo (City, Zimbabwe) - Population Statistics, Charts, Map and Location.  
792 <http://citypopulation.info/php/zimbabwe-admin.php?adm1id=A>.
- 793 57. Melegaro, A. *et al.* Social Contact Structures and Time Use Patterns in the Manicaland Province  
794 of Zimbabwe. *PLOS ONE* **12**, e0170459 (2017).
- 795 58. Kucharski, A. J., Conlan, A. J. K. & Eames, K. T. D. School's Out: Seasonal Variation in the  
796 Movement Patterns of School Children. *PLOS ONE* **10**, e0128070 (2015).
- 797 59. Zhang, J. *et al.* Patterns of human social contact and contact with animals in Shanghai, China.  
798 *Sci. Rep.* **9**, 1–11 (2019).



## Extended Data

# Age-dependent effects in the transmission and control of COVID-19 epidemics

Authors: Nicholas G. Davies<sup>1\*</sup>, Petra Klepac<sup>1^</sup>, Yang Liu<sup>1^</sup>, Kiesha Prem<sup>1</sup>, Mark Jit<sup>1</sup>, CMMID COVID-19 working group, Rosalind M Eggo<sup>1\*</sup>

The CMMID COVID-19 working group<sup>1</sup> is: Carl A B Pearson, Billy J Quilty, Adam J Kucharski, Hamish Gibbs, Samuel Clifford, Amy Gimma, Kevin van Zandvoort, James D Munday, Charlie Diamond, W John Edmunds, Rein MGJ Houben, Joel Hellewell, Timothy W Russell, Sam Abbott, Sebastian Funk, Nikos I Bosse, Fiona Sun, Stefan Flasche, Alicia Rosello & Christopher I Jarvis. Order of working group determined at random.

<sup>1</sup> Department of Infectious Disease Epidemiology, London School of Hygiene & Tropical Medicine, Keppel Street, WC1E 7HT

<sup>^</sup> these authors contributed equally

\* correspondence to Rosalind M Eggo [r.eggo@lshtm.ac.uk](mailto:r.eggo@lshtm.ac.uk) or Nicholas G Davies [nicholas.davies@lshtm.ac.uk](mailto:nicholas.davies@lshtm.ac.uk)

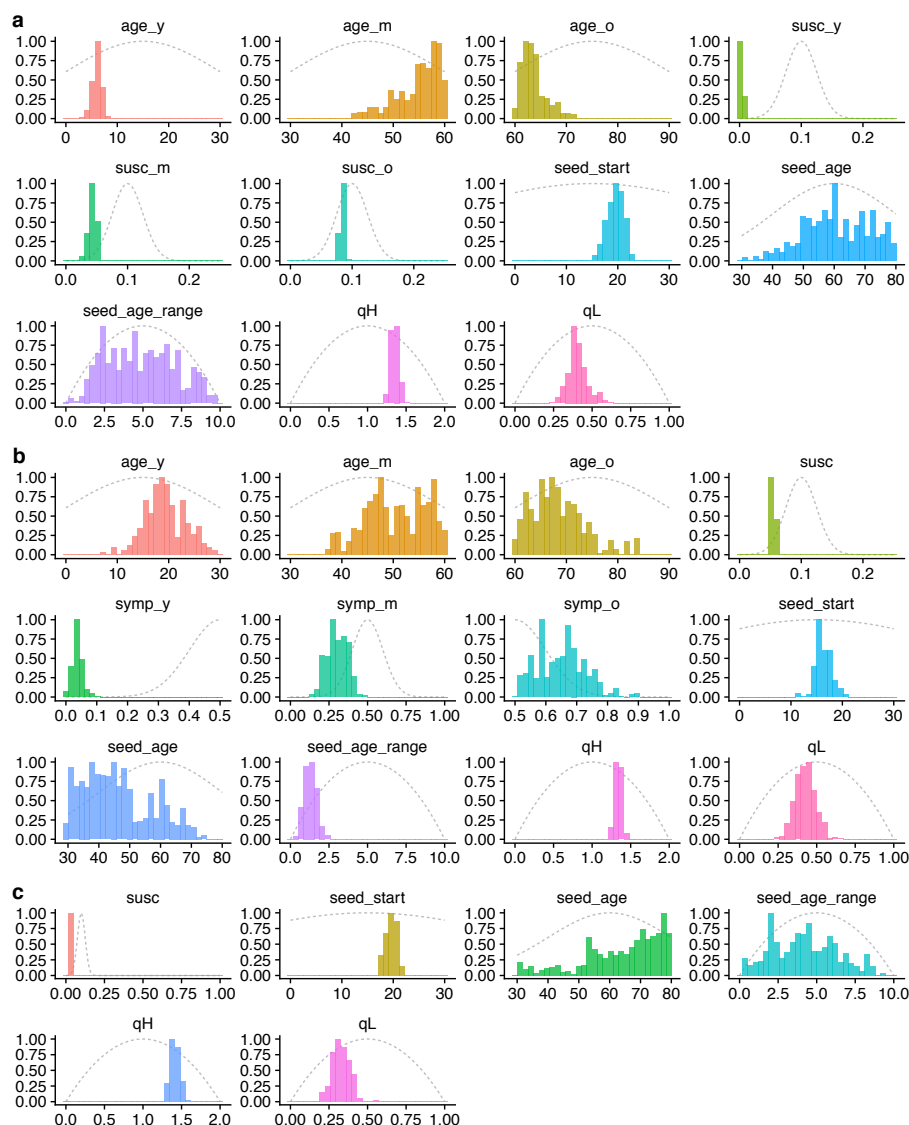


<i>Parameter</i>	<i>Age Group</i>	<i>Mean</i>	<i>Quantile 2.5%</i>	<i>Quantile 25%</i>	<i>Quantile 50%</i>	<i>Quantile 75%</i>	<i>Quantile 97.5%</i>
<i>Susceptibility</i>	0-9	0.33	0.25	0.3	0.33	0.36	0.43
<i>Susceptibility</i>	10-19	0.37	0.28	0.33	0.37	0.4	0.47
<i>Susceptibility</i>	20-29	0.69	0.54	0.64	0.69	0.74	0.82
<i>Susceptibility</i>	30-39	0.81	0.65	0.76	0.81	0.86	0.95
<i>Susceptibility</i>	40-49	0.74	0.59	0.7	0.75	0.79	0.86
<i>Susceptibility</i>	50-59	0.8	0.65	0.76	0.81	0.85	0.93
<i>Susceptibility</i>	60-69	0.89	0.72	0.85	0.9	0.94	0.99
<i>Susceptibility</i>	70+	0.77	0.62	0.72	0.78	0.82	0.9
<i>Clinical fraction</i>	0-9	0.4	0.31	0.36	0.4	0.44	0.48
<i>Clinical fraction</i>	10-19	0.25	0.19	0.23	0.25	0.29	0.32
<i>Clinical fraction</i>	20-29	0.37	0.28	0.33	0.37	0.41	0.46
<i>Clinical fraction</i>	30-39	0.42	0.33	0.38	0.42	0.46	0.51
<i>Clinical fraction</i>	40-49	0.51	0.41	0.47	0.51	0.55	0.6
<i>Clinical fraction</i>	50-59	0.59	0.48	0.55	0.59	0.62	0.67
<i>Clinical fraction</i>	60-69	0.72	0.63	0.69	0.72	0.75	0.79
<i>Clinical fraction</i>	70+	0.76	0.68	0.73	0.76	0.79	0.82

**Extended Data Table 1.** Posterior estimates for the consensus susceptibility and clinical fraction from 6 countries. Note that susceptibility is a relative measure.

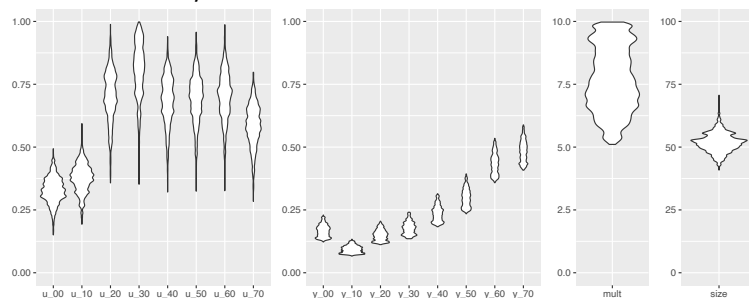
Parameter	Description	Applies in fits	Value	Reference
$d_E$	Incubation period (E to $I_P$ and E to $I_S$ ; days)	All	$\sim \text{gamma}(\mu = 3.0, k = 4)$	Derived from <sup>1</sup> <sub>2</sub>
$d_P$	Duration of preclinical infectiousness (days)	All	$\sim \text{gamma}(\mu = 2.1, k = 4)$	Derived from <sup>2</sup>
$d_C$	Duration of clinical infectiousness ( $I_C$ to R; days)	All	$\sim \text{gamma}(\mu = 2.9, k = 4)$	<sup>3</sup>
$d_S$	Duration of subclinical infectiousness (days)	All	$\sim \text{gamma}(\mu = 5, k = 4)$	Assumed
$u_i$	Susceptibility for age group $i$	Varies by age in Wuhan hypothesis 2, otherwise all ages equal	Estimated	
$y_i$	Probability of clinical infection for age group $i$	Varies by age in Wuhan hypothesis 3, otherwise all ages equal	Either fixed (50%) or estimated	<sup>4</sup>
$f$	Relative infectiousness of subclinical cases	All	50% (0% and 100% in sensitivity analysis)	Assumed
$c_{ij}$	Number of age- $j$ individuals contacted by an age- $i$ individual per day	All	Country-specific contact matrix (sensitivity analysis using synthetic matrices <sup>19</sup> )	China <sup>32</sup> ; UK <sup>7</sup> ; Zimbabwe <sup>34</sup>
$N_i$	Number of age- $i$ individuals	All	Demographic data	<sup>5</sup>
$\Delta t$	Time step for discrete-time simulation	All	0.25 days	
$A_{min}, A_{max}$	Age range of seed cases	Wuhan	Estimated	
$t_{seed}$	Day upon which seeding of infections starts	All	Estimated	
$q_H$	Relative change in non-school contacts during lunar new year holidays	Wuhan	Estimated	
$q_L$	Relative change in non-school contacts following large-scale restrictions	Wuhan, South Korea, Shanghai, Beijing, Italy	Estimated	
$t_L$	Day upon which large-scale restrictions start	Wuhan, South Korea, Shanghai, Beijing, Italy	Fixed to January 23 for Wuhan; estimated for other settings	

**Extended Data Table 2.** Model parameters.

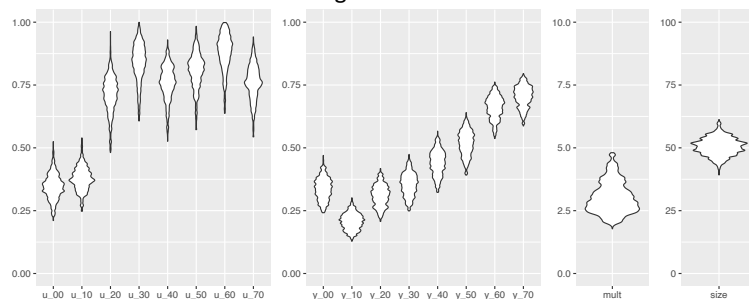


**Extended Data Figure 1.** Prior distributions (grey dotted lines) and posterior distributions (coloured histograms) for model parameters fitting to the early epidemic in Wuhan (Fig. 1, main text); seed\_start is measured in days after November 1st, 2019. **(a)** Model 1 (age-varying contact patterns and susceptibility); **(b)** Model 2 (age-varying contact patterns and clinical fraction); **(c)** Model 3 (age-varying contact patterns only). See also Supplementary Table 3.

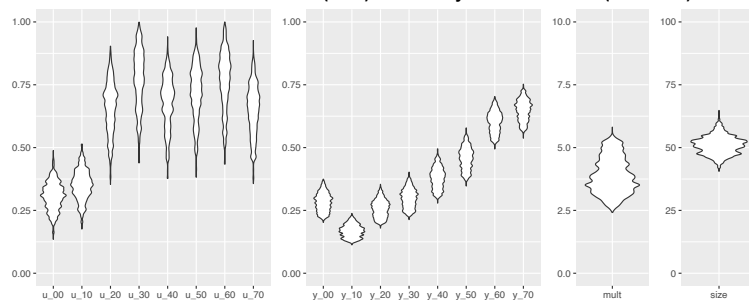
Riccardo et al. only



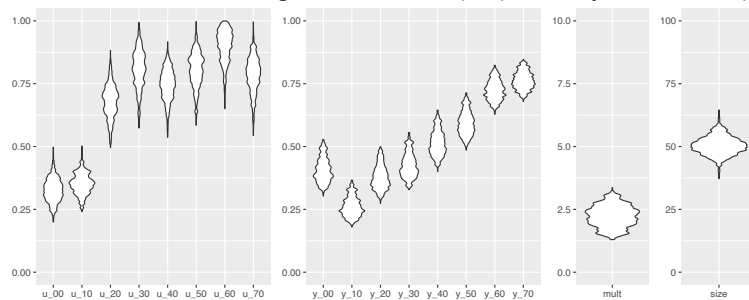
Riccardo et al. + Bi et al. & Zhang et al.



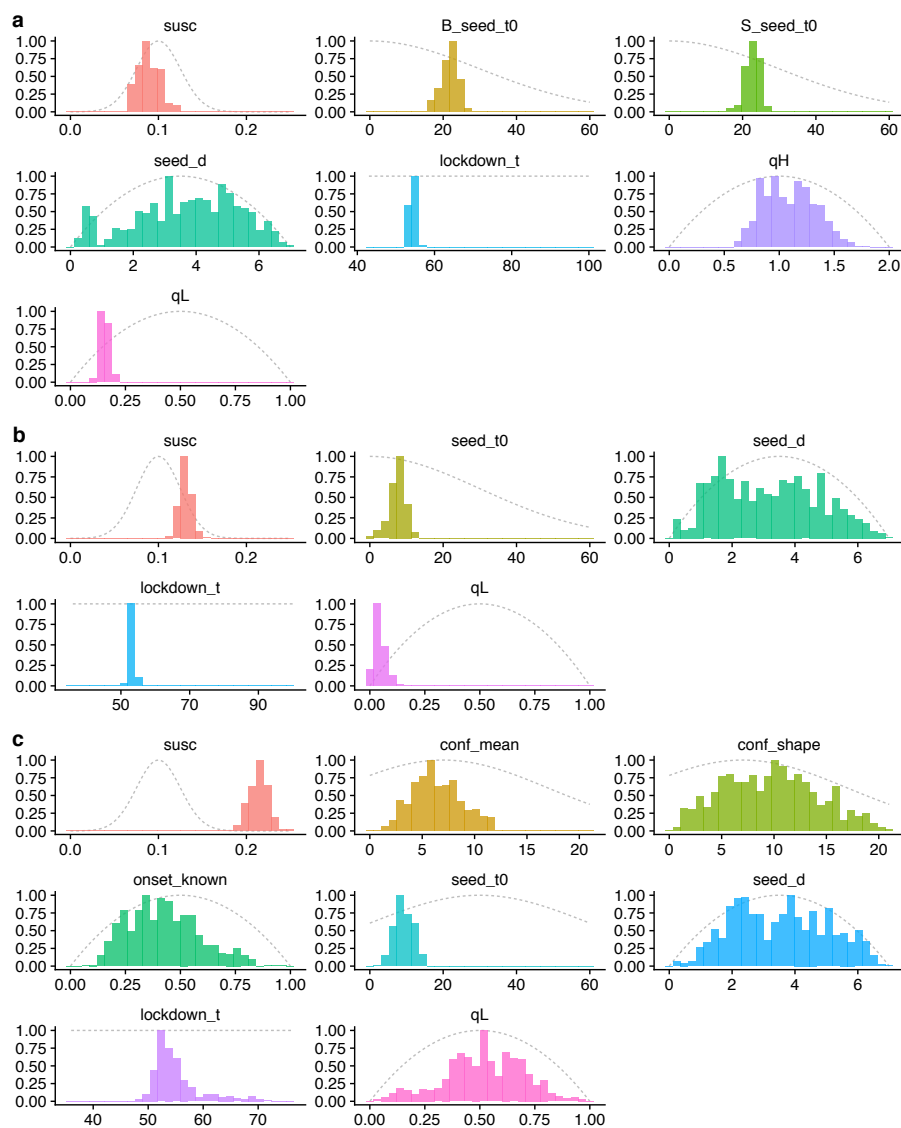
Riccardo et al. + Lavezzo et al. (Vo') & Gudbjartsson et al. (Iceland)



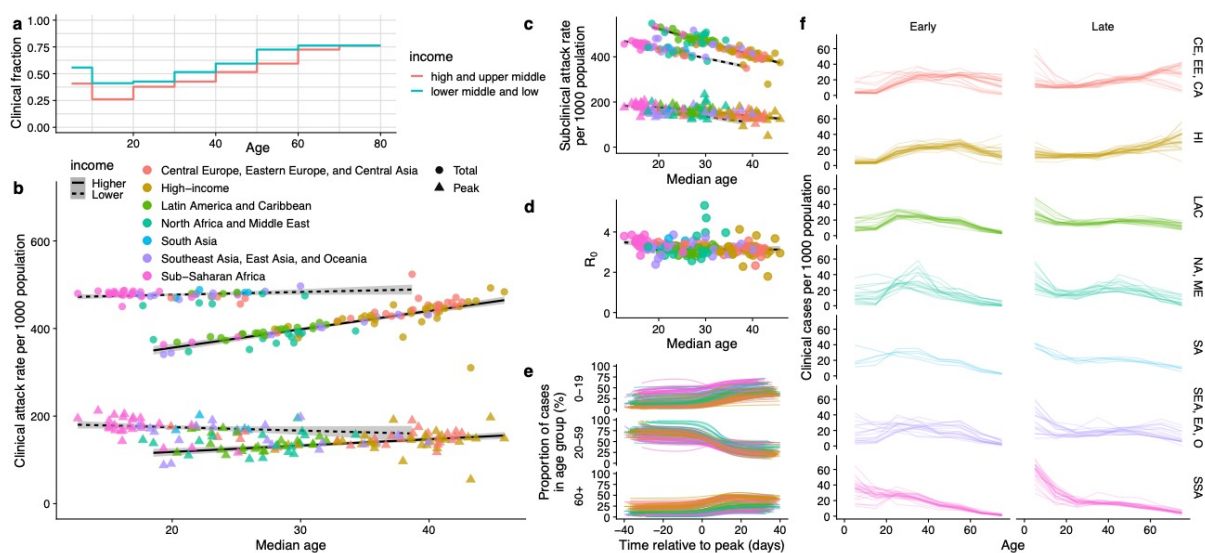
Riccardo et al. + Bi & Zhang + Lavezzo et al. (Vo') & Gudbjartsson et al. (Iceland)



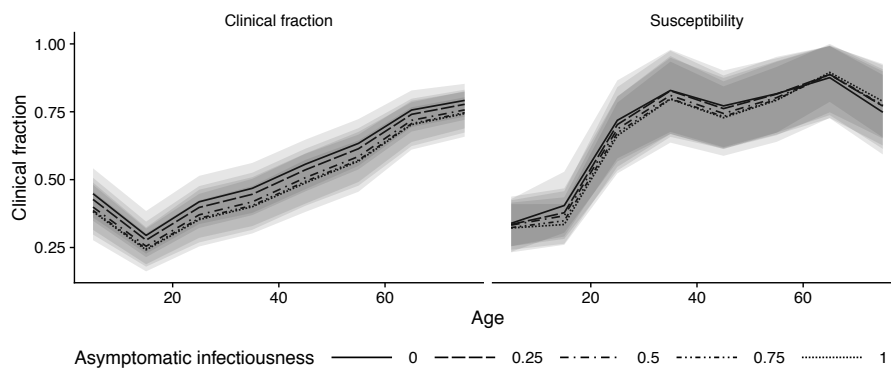
**Extended Data Figure 2.** Analysis showing how the inferred age-varying susceptibility (first column) and age-varying clinical fraction (second column) depend upon the additional data sources used.



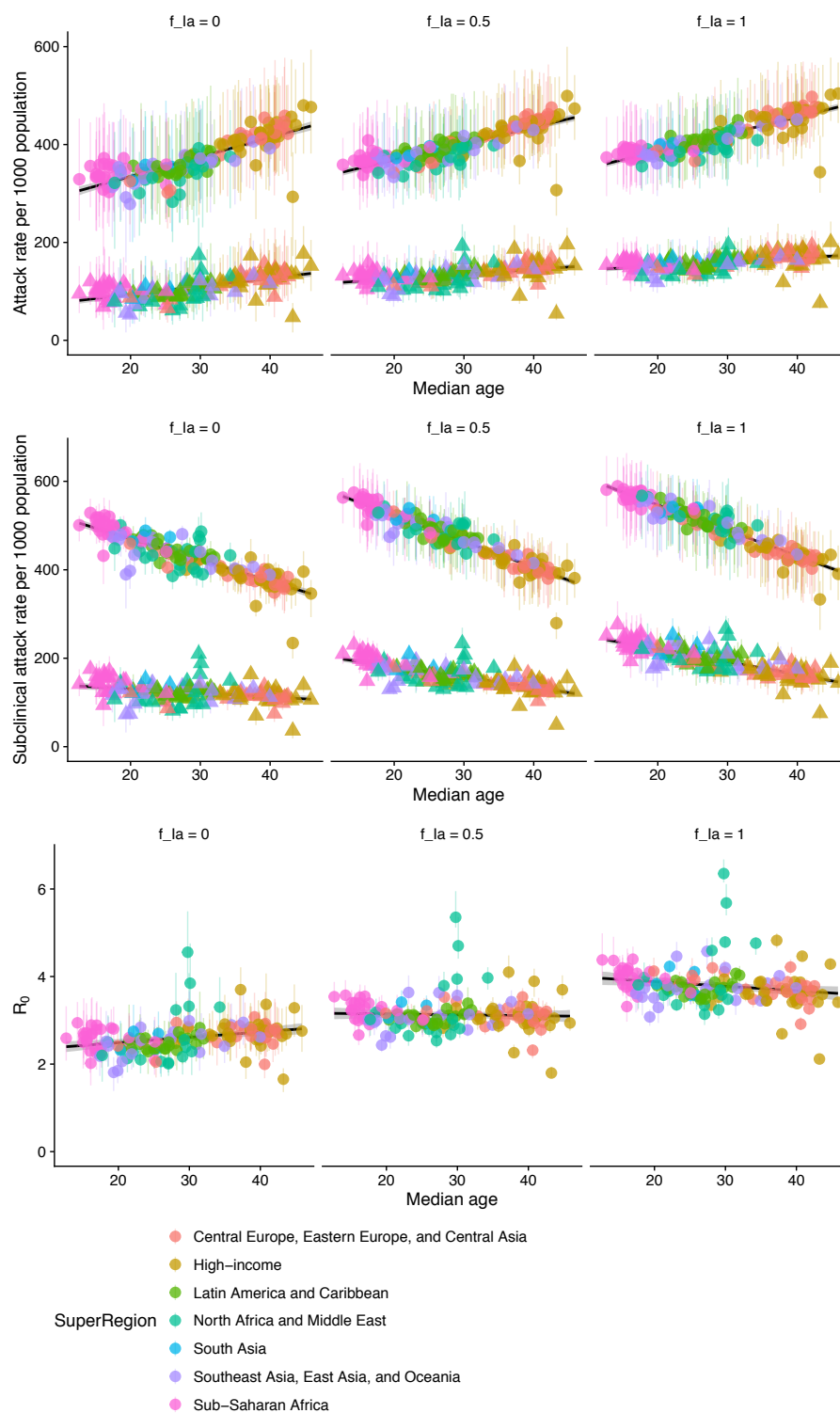
**Extended Data Figure 3.** Prior and posterior distributions for the epidemics in **(a)** Beijing and Shanghai, **(b)** South Korea and **(c)** Lombardy using the “consensus” fit for age-specific clinical fraction and assuming subclinical infections are 50% as infectious as clinical infections (see Fig. 2c, main text). For **(a)**, times are in days after December 1st, 2019; for **(b)** and **(c)**, times are in days after January 1st, 2019. Note, seed\_d is the inferred duration of the seeding event. See also Supplementary Table 3.



**Extended Data Figure 4.** Global projections assuming greater severity in lower-income countries. **(a)** Schematic age-specific clinical fraction for higher-income and lower-income countries. **(b-f)** Illustrative results of the projections for 146 capital cities assuming a higher age-varying clinical fraction in lower-income countries. See Fig. 4 (main text) for details.

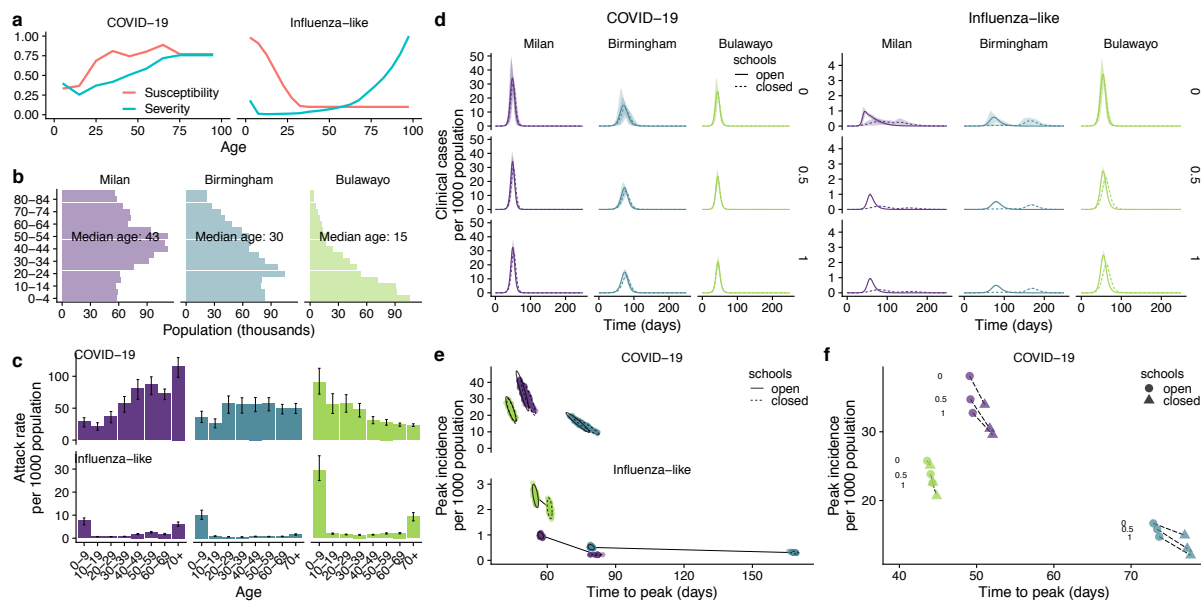


**Extended Data Figure 5.** Consensus age-specific clinical fraction and susceptibility, assuming subclinical infections are 0%, 25%, 50%, 75%, or 100% as infectious as clinical infections.

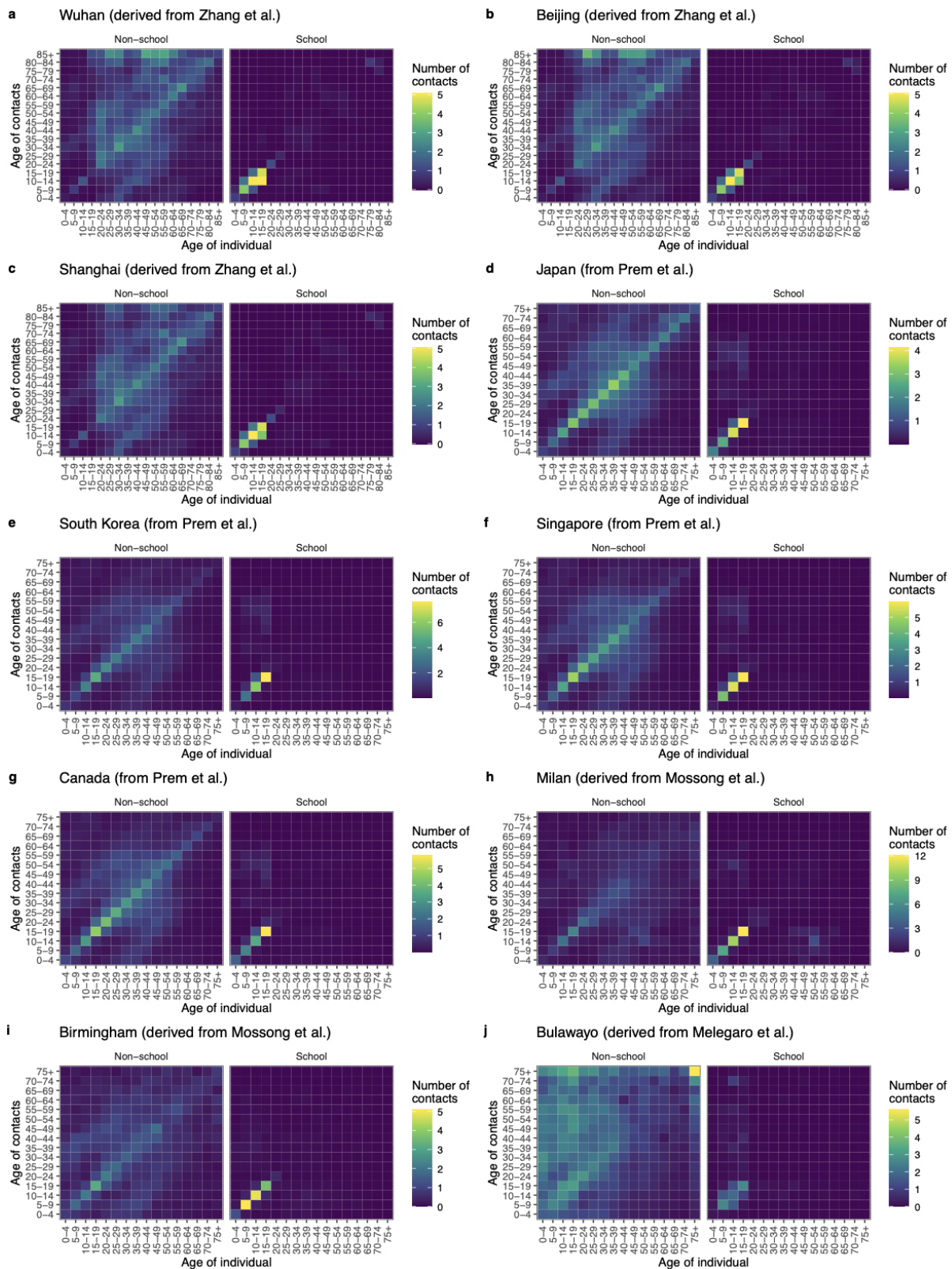


**Extended Data Figure 6.** (a) Projected total and peak clinical case attack rate for 146 capital cities, under different assumptions for the infectiousness of subclinical infections. (b) Projected total and peak subclinical infection attack rate for 146 capital cities, under different assumptions for the infectiousness of subclinical infections. (c) Projected differences in  $R_0$  among 146 capital cities, under different assumptions for the infectiousness of subclinical infections.





**Extended Data Figure 7.** Comparison of school closures in three exemplar cities when susceptibility  $u_i$  is fixed across settings instead of  $R_0$ .



**Extended Data Figure 8.** Contact matrices used for Figs. 1-3 of the main text. We have not shown matrices for all 12 regions of Italy modelled, nor for all 13 provinces of China modelled, as these show similar patterns to the matrices for Milan and for Wuhan, Beijing and Shanghai, respectively.

## Supplementary Information

# Age-dependent effects in the transmission and control of COVID-19 epidemics

Authors: Nicholas G. Davies<sup>1\*</sup>, Petra Klepac<sup>1^</sup>, Yang Liu<sup>1^</sup>, Kiesha Prem<sup>1</sup>, Mark Jit<sup>1</sup>, CMMID COVID-19 working group, Rosalind M Eggo<sup>1\*</sup>

The CMMID COVID-19 working group<sup>1</sup> is: Carl A B Pearson, Billy J Quilty, Adam J Kucharski, Hamish Gibbs, Samuel Clifford, Amy Gimma, Kevin van Zandvoort, James D Munday, Charlie Diamond, W John Edmunds, Rein MGJ Houben, Joel Hellewell, Timothy W Russell, Sam Abbott, Sebastian Funk, Nikos I Bosse, Fiona Sun, Stefan Flasche, Alicia Rosello & Christopher I Jarvis. Order of working group determined at random.

<sup>1</sup> Department of Infectious Disease Epidemiology, London School of Hygiene & Tropical Medicine, Keppel Street, WC1E 7HT

<sup>^</sup> these authors contributed equally

\* correspondence to Rosalind M Eggo [r.eggo@lshtm.ac.uk](mailto:r.eggo@lshtm.ac.uk) or Nicholas G Davies [nicholas.davies@lshtm.ac.uk](mailto:nicholas.davies@lshtm.ac.uk)

Parameter	Description	Prior
$u_i$	Susceptibility to infection upon contact with an infectious person	<p>Non-age-varying: <math>u_i \sim normal(\mu = 0.1, \sigma = 0.025, min = 0)</math></p> <p>Age-varying: young, middle, and old age fit as  <math>a_y \sim normal(\mu = 15, \sigma = 15, min = 0, max = 30)</math>  <math>a_m \sim normal(\mu = 45, \sigma = 15, min = 30, max = 60)</math>  <math>a_o \sim normal(\mu = 75, \sigma = 15, min = 60, max = 90)</math></p> <p>Susceptibility for young, middle, and old age fit as  <math>u_y \sim normal(\mu = 0.1, \sigma = 0.025, min = 0)</math>  <math>u_m \sim normal(\mu = 0.1, \sigma = 0.025, min = 0)</math>  <math>u_o \sim normal(\mu = 0.1, \sigma = 0.025, min = 0)</math></p> <p>Then  <math>u_i = coss(i a_y, b_y, a_m, b_m, a_o, b_o)</math> (see final row)</p>
$y_i$	Clinical fraction on infection	<p>Non-age-varying: <math>y_i = 0.5</math></p> <p>Age-varying: young, middle, and old age fit as  <math>a_y \sim normal(\mu = 15, \sigma = 15, min = 0, max = 30)</math>  <math>a_m \sim normal(\mu = 45, \sigma = 15, min = 30, max = 60)</math>  <math>a_o \sim normal(\mu = 75, \sigma = 15, min = 60, max = 90)</math></p> <p>Susceptibility for young, middle, and old age fit as  <math>y_y \sim normal(\mu = 0.5, \sigma = 0.1, min = 0, max = 0.5)</math>  <math>y_m = 0.5</math>  <math>y_o \sim normal(\mu = 0.5, \sigma = 0.1, min = 0.5, max = 1)</math></p> <p>Then  <math>y_i = coss(i a_y, y_y, a_m, y_m, a_o, y_o)</math> (see below)</p>
$t_{seed}$	Timing of introduction of cases	$t_{seed} \sim normal(\mu = 15, \sigma = 30, min = 0, max = 30)$
$q_H$	Multiplicative factor for transmission during holiday period	$q_H \sim beta(\alpha = 2, \beta = 2)$ scaled to 0 – 2
$q_L$	Multiplicative factor for transmission during large-scale restrictions	$q_L \sim beta(\alpha = 2, \beta = 2)$
$A_{min}, A_{max}$	Age bounds for introduced cases	$A \sim normal(\mu = 60, \sigma = 20, min = 40, max = 80)$ $A_{range} \sim beta(\alpha = 2, \beta = 2)$ scaled to 0 – 10 $A_{min} = A - A_{range}$ $A_{max} = A + A_{range}$
$coss(a x_1, y_1, x_2, y_2, x_3, y_3)$	Cosine-smoothing function	For a given age $a$ (the midpoint age of age group $i$ ) the function evaluates to $y_1$ for $a \leq x_1$ , to $y_2$ for $a = x_2$ , and to $y_3$ for $a \geq x_3$ . Values of $a$ between $x_1$ and $x_2$ are interpolated between $y_1$ and $y_2$ , and values of $a$ between $x_2$ and $x_3$ are interpolated between $y_2$ and $y_3$ , where the interpolation takes the shape of a cosine curve between $-\pi$ and $\pi$ .

Supplementary Table 1. Details of model fitting.

Location	Mixing matrix details
Wuhan City, China	We used mixing matrices measured in Shanghai in 2017/2018 <sup>6</sup> , adapted to the demographics of Wuhan prefecture. This implicitly assumes that Shanghai mixing patterns are representative of large cities in China.
Regions of China: Anhui, Guangdong, Guangxi, Hubei, Hunan, Jiangsu, Jiangxi, Jilin Shaanxi, Shandong, Sichuan, Tianjin, Zhejiang provinces; Beijing, Shanghai.	We used mixing matrices measured in Shanghai in 2017/2018 <sup>6</sup> , adapted to the demographics of each province / city.
Regions of Italy: Lombardia, Piemonte, Trento Veneto, Friulli Venezia Giulia, Liguria, Emilia-Romagna, Toscana, Marche, Lazio, Campania, Puglia regions; Milan.	We used mixing matrices measured in Italy in 2005/2006 <sup>7</sup> , adapted to the demographics of each region / city. This assumes that these contact patterns will still be representative of contact patterns in 2020.
Ontario, Canada	We used synthetic contact matrices, generated based on demographic information about the country <sup>8</sup> .
Japan	We used synthetic contact matrices, generated based on demographic information about the country <sup>8</sup> .
Singapore	We used synthetic contact matrices based on demographic information about the country <sup>8</sup> .
South Korea	We used synthetic contact matrices based on demographic information about the country <sup>8</sup> .
Birmingham, UK	We used mixing matrices measured in the UK in 2005/2006 <sup>7</sup> , adapted to the demographics of Birmingham. This assumes that these contact patterns will still be representative of contact patterns in 2020.
Bulawayo, Zimbabwe	We used mixing matrices measured in Manicaland, Zimbabwe in 2013 <sup>9</sup> , adapted to the demographics of Bulawayo. This implicitly assumes that Manicaland mixing patterns are representative of Bulawayo.
150 capital cities	We used synthetic contact matrices, generated based on demographic information about each country <sup>8</sup> .

**Supplementary Table 2.** Details on mixing matrices used in the study.

Wuhan: Model 1		
age_y	6	(4.2-7.2)
age_m	55	(46-60)
age_o	64	(60-68)
susc_y	0.003	(0.00014-0.0076)
susc_m	0.044	(0.032-0.054)
susc_o	0.084	(0.079-0.09)
seed_start	19	(16-22)
seed_age	61	(42-79)
seed_age_range	4.9	(1.5-8.9)
qH	1.4	(1.3-1.5)
qL	0.41	(0.3-0.56)
Wuhan: Model 2		
age_y	19	(14-29)
age_m	50	(40-60)
age_o	68	(60-79)
susc	0.055	(0.052-0.059)
symp_y	0.037	(0.0051-0.062)
symp_m	0.3	(0.19-0.42)
symp_o	0.65	(0.52-0.77)
seed_start	16	(14-20)
seed_age	46	(30-67)
seed_age_range	1.3	(0.5-1.9)
qH	1.3	(1.2-1.4)
qL	0.43	(0.31-0.56)
Wuhan: Model 3		
susc	0.046	(0.045-0.048)
seed_start	20	(17-21)
seed_age	64	(37-80)
seed_age_range	4.2	(0.93-8.7)
qH	1.4	(1.3-1.5)
qL	0.33	(0.21-0.42)
Beijing, Shanghai		
susc	0.062	(0.05-0.077)
B_seed_t0	18	(8.7-23)
S_seed_t0	19	(12-25)
seed_d	3.1	(0.74-6.3)
lockdown_t	54	(53-56)
qH	1.3	(0.89-1.8)
qL	0.19	(0.15-0.25)
South Korea		
susc	0.098	(0.087-0.11)
seed_t0	9.2	(4.9-13)
seed_d	3.3	(0.73-6)
lockdown_t	53	(52-54)
qL	0.052	(0.0011-0.1)
Lombardy		
susc	0.084	(0.075-0.096)
conf_mean	7.6	(2.7-13)
conf_shape	11	(3.7-20)
onset_known	0.36	(0.061-0.62)
seed_t0	15	(11-20)
seed_d	3.6	(0.83-6.3)
lockdown_t	50	(47-54)
qL	0.48	(0.28-0.72)

**Supplementary Table 3.** Posterior means and 95% HDIs from fitting the dynamic transmission model (Figs. 1 and 2, main text).